

Fast and Accurate Node-Age Estimation Under Fossil Calibration Uncertainty Using the Adjusted Pairwise Likelihood

Greg M. Ellison¹, Liang Liu^{1,*}, ¹ *Department of Statistics, University of Georgia, Athens, 30601, USA*

**Correspondance should be sent to LL. Email: lliu@uga.edu*

December 3, 2025

Abstract

Estimating divergence times from molecular sequence data is central to reconstructing the evolutionary history of lineages. Although Bayesian relaxed-clock methods provide a principled framework for incorporating fossil information, their dependence on repeated evaluations of the full phylogenetic likelihood makes them computationally demanding for large genomic datasets. Furthermore, because disagreements in divergence-time estimates often arise from uncertainty or error in fossil placement and prior specification, there is a need for methods that are both computationally efficient and robust to fossil-calibration uncertainty. In this study, we introduce fast and accurate alternatives based on the phylogenetic pairwise composite likelihood, presenting two adjusted pairwise likelihood (APW) formulations that employ asymptotic moment-matching weights to better approximate the behavior of the full likelihood within a Bayesian MCMC framework. Extensive simulations across diverse fossil-calibration scenarios show that APW methods produce node-age estimates comparable to those obtained from the full likelihood while offering greater robustness to fossil misplacement and prior misspecification, due to the reduced sensitivity of composite likelihoods to local calibration errors. Applied to a genome-scale dataset of modern birds, APW methods recover divergence time patterns consistent with recent studies, while reducing computational cost by more than an order of magnitude. Overall, our results demonstrate that adjusted pairwise likelihoods provide a calibration-robust and computationally efficient framework for Bayesian node dating, especially suited for large phylogenomic datasets and analyses in which fossil priors may be uncertain or imperfectly placed.

1 Introduction

Estimating divergence times, often referred to as node-dating, is a foundational task in evolutionary biology. It allows researchers to place evolutionary events on an absolute timescale, transforming phylogenetic trees from representations of relationships into historical narratives of life on Earth (Tamura et al., 2012; Kumar et al., 2022). The molecular clock model (Zuckerkandl and Pauling, 1965; Mulvey et al., 2025) provides a link between sequence evolution and evolution of species on a real time-scale, and carbon dated fossils can be used to calibrate the evolutionary rate of the molecular clock. Although the likelihood function relating the phylogenetic model to the alignment data is expressed in terms of *evolutionary distances* (normalized lengths in units of expected number of mutations per site), information relating mutation rates to real-world time units translates the height of nodes on the tree to real-world time units. Relaxed clock models allow the mutation rates of molecular characters to vary across the tree, for example by assuming the mutation rates at each branch of the tree are independently distributed according to some prior distribution (Drummond et al., 2006; Lepage et al., 2007). Since the node ages and mutation rates are confounded in the likelihood function, accurate estimation of node ages relies on accurate time calibrations using fossil evidence (Dos Reis and Yang, 2012). However, uncertainty about the ages of fossils can introduce considerable uncertainty in estimated divergence times (Rannala and Yang, 2007; Dos Reis and Yang, 2012). Much attention has been given to the role of fossil calibrations in node dating clock analyses, particularly the fact that node age estimates are highly dependent on fossil calibrations (Yang and Rannala, 2005; Heads, 2005; Hug and Roger, 2007; Forest, 2009; Dos Reis and Yang, 2012; Luo et al., 2019; Nguyen and Ho, 2020). Critically, according to the *infinite-sites* theory of Rannala and Yang (2007), uncertainties in the estimates of divergence times do not resolve with more sequence data, and the quality of node age estimates is highly dependent on the quality of fossil information used to calibrate the node ages.

Bayesian methods are commonly used for node-dating due to their ability to incorporate prior information in the form of fossils calibrations. One or more fossils are placed at nodes of the tree topology to constrain the topology according to the ancestral relationship of the fossil to sampled taxa and a prior distribution is placed on the node age according to evidence the fossil age (Parham et al., 2011). In this way, a prior distribution is imposed on the ages of all nodes, and the prior information is used to disentangle the divergence times and mutation rates (Inoue et al., 2009; Yang, 2014a; Nascimento et al., 2017). Inference about node ages is made by examining posterior credible sets of node ages samples from the MCMC chain; the tree topology is often assumed fixed, so no problems arise from needing to consider nodes only present in some sampled tree topologies, although with MCMC sampling it is possible to integrate out the uncertainty due to the unknown topology by sampling from the tree topology posterior distribution. A well-known limitation of the fully Bayesian approach is the substantial computational burden created by repeated likelihood evaluations along long MCMC chains. MCMCTree addresses this issue by employing a likelihood approximation to accelerate computation (Rannala and Yang, 2007; Reis and Yang, 2011), yet the method remains computationally demanding for datasets with long sequences, a difficulty shared by other widely used programs such as MrBayes (reference) and BEAST2 (reference). The challenge has become even more pronounced with the proliferation of high-throughput sequencing technologies, which produce large-scale genomic datasets for phylogenetic inference (Liu et al., 2015; Patané et al., 2017; Young and Gillung, 2019). Although likelihood-based approaches, including both maximum likelihood and Bayesian inference, remain the statistical gold standard due to their desirable theoretical properties and principled frameworks for model selection and parameter estimation, their computational requirements can be prohibitive for large phylogenies with many taxa or extensive sequence data.

Composite likelihoods have become popular for their ease of construction and computation (Varin, 2008; Varin et al., 2011). The pairwise composite likelihood, for example, constructs an approximate likelihood by combining marginal likelihoods of pairs of data; in the case of a DNA sequence alignment of M taxa, this likelihood is computed by considering only pairs of nucleotides rather than the full site patterns of M characters. This approach can result in a considerable computational advantage, although it has theoretical drawbacks due to ignoring the state of ancestral sequences and the dependency among sequences (Farris, 1985; Steel, 2009). However, methods have been developed to mitigate the drawbacks that arise when using the composite likelihood as a misspecified likelihood function (Varin, 2008; Varin et al., 2011), including in the Bayesian setting (Pauli et al., 2011; Ribatet et al., 2012; Shaby, 2014; Miller, 2021); as the marginal likelihoods that comprise the pairwise likelihood are valid likelihoods themselves, the composite pairwise likelihood retains good estimation properties. Adjustment weights based on asymptotic properties of the composite Likelihood Ratio Test (LRT) statistic are often used to correct the composite likelihood, and result in improved parameter estimation relative to the unadjusted

composite likelihood (Pauli et al., 2011; Ribatet et al., 2012; Cattelan and Sartori, 2015). The pairwise likelihood has been studied previously for phylogeny inference (Holder and Steel, 2011; Wu and Susko, 2009, 2010), and recent works including Peng et al. (2022) and Kong et al. (2024) have applied composite likelihood methods to tree estimation under the multi-species coalescent and use of phylogenetic networks to efficiently estimate tree topologies in the presence of hybridization, respectively. Liu et al. (2010) was the first paper to use the composite likelihood to estimate species trees under the multi-species coalescent model.

For large sequence datasets, we propose a Bayesian divergence-time framework that replaces the full phylogenetic likelihood with a pairwise composite likelihood. Since the pairwise likelihood involves a number of terms proportional to $c^2 \binom{M}{2}$, where M denotes the number of taxa and c the number of character states in the substitution model, its computational cost does not scale with sequence length. In contrast, the full phylogenetic likelihood becomes increasingly expensive as alignments grow longer. The pairwise composite likelihood therefore offers a computationally efficient alternative for analyses based on long sequence alignments. In this study, we introduce adjusted pairwise (APW) likelihoods and demonstrate that they enable fast and accurate estimation of divergence times. We assess the performance of the APW approach using a comprehensive simulation study modeled on the node-age analysis of modern birds by Wu et al. (2024a). Although the avian tree of life has been examined extensively over the past two decades (Hackett et al., 2008; Jarvis et al., 2014; Prum et al., 2015; Wu et al., 2024a), the divergence between modern birds (*Neoaves*) and flightless birds (*Paleognathae*) remains contentious, due in part to the placement and uncertainty of fossil calibrations (Claramunt et al., 2024; Wu et al., 2024b). Across a wide range of fossil-calibration scenarios, our simulations show that APW methods produce node-age estimates comparable to those obtained from the full likelihood while exhibiting greater robustness to fossil misplacement and prior misspecification. This robustness arises from the reduced sensitivity of composite likelihoods to local calibration errors. These results demonstrate that APW likelihoods provide a calibration-resilient and computationally efficient framework for Bayesian node dating.

2 Background

2.1 Composite likelihoods

Suppose data $X = \{X_i, i = 1, \dots, n\}$, are independently generated from the probability distribution f parameterized by the vector $\theta \in \Theta$. Further suppose $\theta = (\phi, \gamma)$, where ϕ is a p dimensional vector of parameters of interest and γ is a k dimensional vector of nuisance parameters. The likelihood of θ is the joint distribution of the data, $f(X|\theta)$, viewed as a function of the parameters and is referred to as the *full* likelihood function. The *composite* likelihood is an approximate likelihood function constructed by treating the marginal likelihoods of subsets of the data as independent (Lindsay, 1988; Varin et al., 2011). For marginal events $(A_s), s = 1, \dots, S$, let $f_s(\theta|X) \propto f(\theta|X \in A_s)$ be the marginal likelihood of A_s . Then the composite marginal likelihood is defined as $f_c = \prod_s f_s(\theta|X)$. Under typical regularity conditions, a central limit theorem ensures the composite likelihood maximum likelihood estimator is asymptotically normal, with covariance matrix $G(\theta)^{-1}$, where G is defined below (Varin et al., 2011). In the phylogenetic setting, (Holder and Steel, 2011) show that the maximum pairwise likelihood estimates are consistent for the tree topology and branch lengths.

In the Bayesian setting, the parameters are viewed as random, and inference is made by sampling parameter values from the posterior distribution of the parameters given the observed data. Given prior $\pi(\theta) = \pi(\phi)\pi(\gamma)$ (assumed to be a proper prior), we denote the typical posterior distribution $\pi(\theta|X) \propto f_c(\theta|X)\pi(\theta)$ and as the composite posterior distribution

$$\pi_c(\theta|X) = \frac{f_c(\theta|X)\pi(\theta)}{\int_{\Theta} f_c(\theta|X)\pi(\theta)d\theta}. \quad (1)$$

The construction of the composite likelihood treats the marginal likelihoods as independent components, ignoring any higher-order dependence structure captured by the full likelihood function. Thus, there is a loss of information due to use of the composite likelihood relative to the full likelihood, and credible sets obtained from posterior distributions based on composite likelihoods may not provide reasonable coverage probabilities of parameters of interest. Pauli et al. (2011) and Ribatet et al. (2012) apply composite likelihoods to Bayesian inference of spatial extreme models, and adjust the resulting posteriors to recover approximate frequentist asymptotic properties of the composite likelihood. Shaby (2014) finds a similar adjustment with exact frequentist coverage properties, and Wu and Ghosh (2017)

derive a Bernstein-Von Mises theorem from the composite posterior. Miller (2021) unites various similar approaches with the idea with the notion of *Generalized Posteriors*, and formalizes regularity conditions for generalized posterior concentration, asymptotic normality, and frequentist coverage set properties. Inference for θ based on the composite likelihood, denoted $f_c(\theta|X)$ is often justified via asymptotic results of likelihood ratio test statistics (Rotnitzky and Jewell, 1990; Chandler and Bate, 2007). Strategies to adjust the composite likelihood typically make use of the asymptotic distribution of the composite likelihood ratio test (LRT) statistic (Geys et al., 1999; Varin, 2008; Chandler and Bate, 2007) to derive a weight for the composite likelihood; we discuss the weights in more detail below, and for now define an adjusted pairwise likelihood (APW) as $f_c^a(\theta|X) = f_c(\theta|X)^w$ for some adjustment weight $w > 0$, with corresponding log-likelihood $\ell_c^a = w \ln f_c(\theta|X)$.

To discuss the asymptotic properties of estimates based on the composite posterior, we denote the ‘true’ values of the parameters $\theta_0 = (\phi_0, \gamma_0)$. We also denote the maximum composite likelihood estimator $\hat{\theta}_c$, defined as $\hat{\theta}_c = \underset{\theta}{\operatorname{argmax}} \ell_c(\theta)$, where $\ell_c(\theta)$ is the logarithm of the composite likelihood. We define the composite score function $u_c(\theta) = \nabla_{\theta} \ell_c(\theta)$, and matrices $J(\theta) = E_X[u_c(\theta)'u_c(\theta)]$ and $H(\theta) = -E_X[\nabla_{\theta} u_c(\theta)]$, respectively referred to as the *sensitivity* and *variability* matrices. Since the estimate is from a linear combination of the data margins and not the full likelihood, $J(\theta_0) \neq H(\theta_0)$, and composite likelihood asymptotic theory requires the *Godambe Information Matrix* $G(\theta_0) = H(\theta_0)J^{-1}(\theta_0)H(\theta_0)$. If interest is on the parameters ϕ , partition the matrices

$$H(\theta_0) = \begin{bmatrix} H_{\phi\phi} & H_{\phi\gamma} \\ H_{\gamma\phi} & H_{\gamma\gamma} \end{bmatrix} \text{ and } H(\theta_0)^{-1} = \begin{bmatrix} H^{\phi\phi} & H^{\phi\gamma} \\ H^{\gamma\phi} & H^{\gamma\gamma} \end{bmatrix},$$

where H_{γ} refers to the block of the partitioned matrix M corresponding to the parameter γ . For testing parameter value θ_0 the composite LRT statistic is defined as $\Lambda_c = -2(\ell_c(\hat{\theta}_c) - \ell_c(\theta_0))$; which has asymptotic distribution $\sum_{i=1}^p \lambda_i Z_i^2$, where Z_i^2 are independent chi-square random variables and the λ_i are the eigenvalues of $(H^{\phi\phi})^{-1}G^{\phi\phi}$, calculated under the null hypothesis. Here, $G^{\phi\phi}$ is the submatrix of the inverse of $G(\theta_0)$ which corresponds to the parameter ϕ . In the case that $\theta = \phi$, this simplifies to $H^{-1}(\theta_0)J(\theta_0)$; from now on we consider only this case. We consider two so-called *magnitude* adjustment weights as described in Ribatet et al. (2012): denoting by λ_i the eigenvalues of $H^{-1}(\theta_0)J(\theta_0)$, the first is $w_1 = p/(\sum_{i=1}^p \lambda_i)$, such that $E[w_1 \Lambda_c] = E[\Lambda]$ (Rotnitzky and Jewell, 1990). The second proposed weight matches the first two moments is $w_2 = \sum_{i=1}^p \lambda_i / \sum_{i=1}^p \lambda_i^2$, such that the composite LRT converges in distribution to χ_{ν}^2 , where $\nu = (\sum_{i=1}^p \lambda_i)^2 / \sum_{i=1}^p \lambda_i^2$ (Varin, 2008). For more possible approaches see, for example, Ribatet et al. (2012) or Shaby (2014). In what follows, we denote the adjusted pairwise likelihoods based on w_1 and w_2 as APW1 and APW2 respectively.

3 Materials and Methods

3.1 Adjusted pairwise likelihood for phylogenetic inference

Given a DNA sequence alignment X consisting of N sites and M taxa, the goal is to estimate the ages, $y = (y_j), j = 1, \dots, y_{M-1}$, of the internal nodes of the tree. We assume a rooted, bifurcated tree topology T is fixed and known. We adopt a *branch-wise* relaxed molecular clock, in which the mutation rate varies across the tree, but is assumed to be constant along each branch (Lepage et al., 2007); we define the model in terms of the branch lengths in units of millions of years, $b = (b_i), i = 1, \dots, 2M - 2$ and overall mutation rate scalar μ .

We assume a substitution model with parameters denoted η . We will consider the *JC* (Jukes and Cantor, 1969) and *GTR* (Tavaré, 1986) substitution models, as the *GTR* model is likely the most commonly employed substitution model in practice, and the *JC* model is the simplest claim above special case of the *GTR* model, in which all relative substitution rates are identical and all nucleotide frequencies are identical. For simplicity in computing the pairwise likelihood weight, we assume the substitution model parameters are fixed and known; in practice, they may be estimated directly from the data and fixed prior to employing the pairwise likelihood adjustment weight. Assuming the substitution model parameters are fixed allows computing the eigenvalues of the simpler matrix $H^{-1}J$ defined above for computing the pairwise likelihood adjustment weight. We assume the site rates follow the Discrete Gamma distribution of (Yang, 1994) with C rate categories and shape parameter α ; we denote the discrete site substitution rates as $(\kappa_i), i = 1, \dots, C$. Because α is not identifiable from the pairwise likelihood for many cases of the *GTR* substitution model (including the *JC* model) (Wu and Susko, 2010), we consider α to be fixed and known when computing the pairwise likelihood.

The composite posterior can be written as

$$f_c(y, \mu, \tau, b, \eta, \delta | X) = \frac{f_c(X | \tau(\mu, b), \eta) f(b | y, \sigma) f(y | \delta) \pi(\tau) \pi(b) \pi(\mu) \pi(y) \pi(\eta)}{m_c(X)},$$

where the pairwise likelihood, defined below, is written as $f_c(X | \tau(\mu, b))$ since the normalized branch lengths are computed as a function of the mutation rate μ and branch lengths b . For convenience, from now on the pairwise likelihood will simply be denoted $f_c(X | \tau, \eta)$. Here, $f(y | \delta)$ is the prior distribution on node ages and $f(b | y, \sigma)$ is the prior distribution on branch lengths b . We employ a birth-death process and independent lognormal branches (Yang and Rannala, 2005; Lepage et al., 2007), and δ and σ represent the hyperparameters associated with these priors. For a more detailed treatment, see (Lepage et al., 2007). The denominator $m_c(X)$ is the marginal data likelihood under the composite likelihood, and is obtained by integrating and summing over the joint parameter space. Inference is made by sampling from the posterior using Markov Chain Monte Carlo (MCMC) methods (Yang and Rannala, 2005; Yang, 2014b).

The alignment matrix is $X = (X_1, \dots, X_M)$, and the full joint distribution of the data given the tree topology and branch lengths is denoted $f(X | \tau, \eta)$. The elements of the alignment matrix X are elements of the character set $\mathcal{X} = (A, C, G, T)$, and we denote by $d = 1, \dots, 16$ the sixteen doublets made up of pairs of characters in \mathcal{X} . The composite pairwise likelihood is defined as $f_c(\tau | X) = \prod_{k=1}^{M-1} \prod_{l=k+1}^M f(X_k, X_l | \tau)$, and the log composite pairwise likelihood is $\ell_c = \ln f_c$. For taxa k define $\mathcal{V}(k, l)$ as the path through the root connecting taxa X_k and X_l . The distance separating sequences X_k and X_l is $\nu_{kl} = \sum_{i \in \mathcal{V}(k, l)} \tau_i$. We also define the set of pairs connected by branch τ_i as $\mathcal{D}_{\tau_i} = \{(k, l) : \tau_i \in \mathcal{V}(k, l)\}$. The observed count of doublet d in pair k, l is denoted n_d^{kl} , and the adjusted pairwise log-likelihood of alignment X is obtained as

$$\ell_c(\tau) = w \sum_{k=1}^{M-1} \sum_{l=k+1}^M \sum_{d=1}^D n_d^{kl} \log(p_d^{kl}),$$

where p_d^{kl} represents the probability of doublet d in sequences separated by distance ν_{kl} and w is the adjustment weight. The weights for the adjusted pairwise likelihoods APW1 and APW2 are defined, respectively, as $w_1 = p / (\sum_{i=1}^p \lambda_i)$ and $w_2 = \sum_{i=1}^p \lambda_i / \sum_{i=1}^p \lambda_i^2$. We refer to the case when $w = 1$ as the PW likelihood.

3.1.1 Estimating J and H

To compute the eigenvalues λ_i , we estimate the matrices $H(\tau_0)$ and $J(\tau_0)$ using independent internal subsets of the alignment following the empirical estimates of Cattelan and Sartori (2015). Given independent subsequences (X_i^s) , $s = 1, \dots, S$, the estimates are

$$\hat{H}_{ij} = \frac{1}{S} \sum_{s=1}^S \sum_{k=1}^{M-1} \sum_{l=k+1}^M \left[\frac{\partial}{\partial \tau_i} \ell_c(\tau | X_{kl}^s) \right] \left[\frac{\partial}{\partial \tau_j} \ell_c(\tau | X_{kl}^s) \right],$$

$$\hat{J}_{ij} = \frac{1}{S} \sum_{s=1}^S \left[\frac{\partial}{\partial \tau_i} \ell_c(\tau; X^s) \right] \left[\frac{\partial}{\partial \tau_j} \ell_c(\tau; X^s) \right].$$

As our application is long concatenated sequence alignments, we expect that typically enough independent internal subsets will be available to estimate the J and H matrices.

Defining the derivatives of the doublet probabilities with respect to the branch lengths by $p_{d,i}^{kl} = \frac{\partial}{\partial \tau_i} p_d^{kl}$, we have

$$\frac{\partial}{\partial \tau_i} \ell_c(\tau | X) = \sum_{(k,l) \in \mathcal{D}_{\tau_i}} \sum_{d=1}^D n_d^{kl} \frac{p_{d,i}^{kl}}{p_d^{kl}},$$

and

$$\frac{\partial}{\partial \tau_i} \ell_c(\tau | X_{kl}) = \begin{cases} \sum_{d=1}^D n_d^{kl} \frac{p_{d,i}^{kl}}{p_d^{kl}} & \text{if } (k, l) \in \mathcal{D}_{\tau_i} \\ 0 & \text{else.} \end{cases}$$

3.1.2 Jukes-Cantor adjustment

For the JC substitution model, all characters are treated identically, so we only consider whether characters at a site are the same or different. There are $D = 2$ possible doublet configurations; identical or differing nucleotides. We use the notation 11 to indicate identical nucleotides and 10 for different nucleotides. The doublet probabilities across distance ν are denoted $p_{10}(\nu)$ and $p_{11}(\nu)$, and refer to the probabilities of observing the same nucleotide or not, respectively. We have $p_{11}(\nu) = \frac{1}{C} \sum_{i=1}^C \left(\frac{1}{4} + \frac{3}{4} e^{-\frac{4}{3} \nu r_c} \right)$, $p_{10}(\nu) = \frac{1}{C} \sum_{i=1}^C \left(\frac{3}{4} - \frac{3}{4} e^{-\frac{4}{3} \nu r_c} \right)$.

$$p_{11,i}^{kl} = \frac{\partial}{\partial \tau_i} p_{11}^{kl} = -\frac{1}{C} \sum_{c=1}^C \kappa_c e^{-\frac{4}{3} \nu_{kl} \kappa_c}$$

$$p_{10,i}^{kl} = \frac{\partial}{\partial \tau_i} p_{10}^{kl} = \frac{1}{C} \sum_{c=1}^C \kappa_c e^{-\frac{4}{3} \nu_{kl} \kappa_c},$$

and the partial derivatives of the PW log likelihood are

$$\frac{\partial}{\partial \tau_i} \ell_c(\tau|X) = \sum_{(k,l) \in \mathcal{D}_{\tau_i}} \sum n_{11}^{kl} \frac{p_{11,i}^{kl}}{p_{11}^{kl}} + n_{10}^{kl} \frac{p_{10,i}^{kl}}{p_{10}^{kl}}.$$

The partial derivatives of the pairwise data marginal likelihoods are

$$\frac{\partial}{\partial \tau_i} \ell_c(\tau|X_{kl}) = \begin{cases} n_{11}^{kl} \frac{p_{11,i}^{kl}}{p_{11}^{kl}} + n_{10}^{kl} \frac{p_{10,i}^{kl}}{p_{10}^{kl}} & \text{if } (k,l) \in \mathcal{D}_{\tau_i} \\ 0 & \text{else.} \end{cases}$$

We estimate τ_0 as

$$\tau_0^{kl} = \begin{cases} -\frac{3}{4} \ln(1 - \frac{4}{3} p^{kl}) & \text{for } JC \\ \alpha \left((1 - \frac{4}{3} p^{kl}) \right)^{-1/\alpha} - 1 & \text{for } JC + \Gamma \end{cases}$$

where $p = \frac{n_{10}^{kl}}{n_{10}^{kl} + n_{11}^{kl}}$.

3.1.3 GTR adjustment

The *GTR* model allows both the relative rates of substitution between pairs of nucleotides $r = (r_{AC}, r_{AG}, r_{AT}, r_{CG}, r_{CT}, r_{GT})$ and relative nucleotide frequencies $\pi = (\pi_A, \pi_C, \pi_G, \pi_T)$ to differ. Given site mutation rate heterogeneity parameter α , the nucleotide transition probabilities along distance ν are given as the elements of the probability transition matrix $P(\nu) = \frac{1}{C} \sum_{c=1}^C e^{Q \nu \kappa_c}$, where Q is the typical *GTR* rate matrix defined such that the off-diagonal elements of Q are the off-diagonal elements of $R\Omega$ where R is the matrix of relative rate parameters and Ω is the diagonal matrix of nucleotide frequencies. The diagonal elements of Q are taken such that the row sums of Q are 0. The doublet probabilities are then calculated as $\Omega P(\nu)$; their derivatives are not available analytically, but may be estimated numerically. We estimate ν_0 for the *GTR* and *GTR* + Γ models using the method of Waddell and Steel (1997) for each taxa pair (k, l) .

3.2 Simulations

We explore the use of the Full, APW1, APW2, and PW likelihoods for Bayesian node dating analysis through extensive simulation studies. Then, we estimate simulated divergence times under the relaxed clock model, with six different fossil calibration settings, as described below.

The simulations use a 15-taxa subtree of the bird tree topology of Wu et al. (2024a). Four of the fossils calibrations are used to calibrate the nodes of the simulation tree, as shown in Figure 1a. The node ages are generated according to birth-death process prior distribution using the default speciation and birth rate parameters in MrBayes. Node ages and branch lengths generated from these prior distributions using an MCMC chain with no data for 5,000,000 generations with no burn-in, and the median sampled node ages are used as the "true" node ages. The overall mutation rate (in units of mutations per millions of years) is assumed to be 0.001, corresponding to 10^{-10} mutations per site per year. The branch-wise mutation rates are sampled from independent log-normal distributions, such that each mutation rate μ_i is drawn independently from a lognormal distribution with mean μ and variance σ^2 (Drummond et al., 2006); the branch lengths in mutation units are then $\tau_i = \mu_i b_i$. We use $\sigma = 0.1$. For all simulations, we simulate alignments of length 1,000, 10,000, and 50,000 using the program **Seq-Gen** (Rambaut and Grass,

1997). For each fossil calibration setting, we simulate 100 independent replicate sequence alignments and estimate the node ages with an MCMC chain of 100,000 generations, discarding the first 50% of samples as burn-in and sampling every 200 generations. The adjustment weights for the APW1 and APW2 likelihoods are computed by splitting the alignment into 5 segments of equal length and taking the elementwise averages of the elements of the J and H matrices from each segment.

To assess the quality of node age estimates we compute the overall root mean square error $rMSE = \frac{1}{RD} \sqrt{\sum_{r=1}^R \sum_i (\hat{d}_i^r - d_i)^2}$, where \hat{d}_i^r is the i th internal node age in the r th simulation, and D is the number of internal nodes. We also compute the posterior credible interval coverage as $\frac{1}{RD} \sum_{r=1}^R \sum_{i=1}^D \mathbb{1}(\hat{d}_{i,0.025}^r < d_i < \hat{d}_{i,0.975}^r)$, where $\hat{d}_{i,p}^r$ is the p th percentile of the sampled posterior values of \hat{d}_i^r . To explore how node age estimation performance changes when node calibration prior distributions are changed, for Calibration Settings $j \neq 1$ we compute the difference in rMSE at a node i between Calibration Setting j and Calibration Setting 1 as $rMSE_j - rMSE_1$ where $rMSE_j = \frac{1}{R} \sqrt{\sum_{r=1}^R (\hat{d}_i^r - d_i)^2}$ with the node age estimates are taken with respect to Calibration Setting j .

3.2.1 Node age estimation

We consider four simulation settings to examine the quality of node-age estimates under different prior distribution calibration settings. In all calibration settings, we use four fossil calibration constraints derived from the bird analysis. The four calibrations consist of two lower bounds on internal nodes set with offset exponential distributions, an interval calibration on the root node set with a uniform distribution, and a calibration on the second oldest node representing the ancestor of the simulation ‘bird’ clade set by an offset lognormal distribution.

The quality of fossils used to calibrate the prior distributions of node ages on the tree is a critical factor in determining the quality of the node age estimates. Placements of fossil calibrations are often disputed, and there is considerable uncertainty inherent to the practice of assigning prior distributions to tree nodes based on the fossil record. We use seven fossil calibration settings to explore the quality of node age estimates obtained from the PW, APW1, APW2 and Full likelihoods. In Calibration Setting 1, all fossils are placed correctly and given prior distributions that are correct for the true node ages. In Settings 2, 3, and 4, all four fossils are correctly placed, but the node ages are calibrated with prior distributions that are misleading about the true node age (as in the case of Setting 2) or less informative about the node ages than Setting 1 (as in Settings 2 and 3). In settings 5, 6, and 7, Fossil 3 is placed incorrectly, but the prior distribution used to calibrate the node age is unchanged. These calibration settings are discussed in more detail below and summarized in Figure 1b. We compare the rMSEs obtained in Setting 1 to the rMSEs obtained in Settings 2-7 to explore the impact of changes in the fossil calibration on the node age estimates obtained by the four likelihoods.

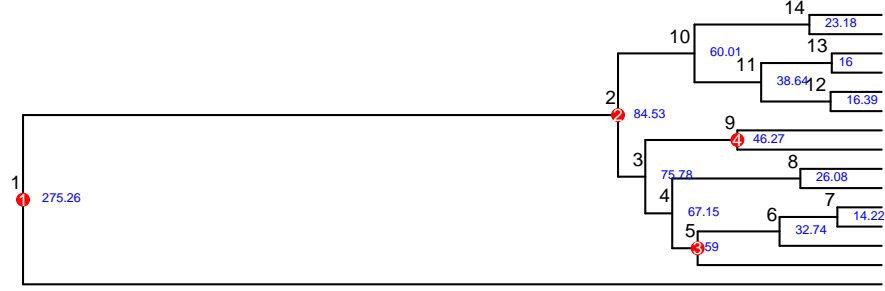
Calibration Setting 1 uses node age calibrations that mimic those used in the bird divergence analysis, as described in the next section. The root node (Node 1) is calibrated with a uniform distribution with lower bound 255.9 MYA and upper bound 299.8 MYA, denoted U(255.9, 299.8). The node representing the modern bird ancestor (Node 2) is calibrated with a lognormal distribution offset to have lower bound 66.7 MYA, mean 81.3 MYA, and standard deviation of 5.3. This is intended to place 2.5% of the distribution’s mass above the ‘soft’ upper bound of 94.1, and is denoted OLN(66.7, 81.3, 5.3). Node 5 is calibrated with an exponential distribution offset to have lower bound 51.6 and mean 72.8, denoted OE(51.6, 72.8) Node 9 is calibrated with an OE(23.3, 61.2) distribution. All calibrations are appropriate for the true node ages.

We conduct additional simulation studies comparing the APW, PW, and Full likelihoods for estimating the branch lengths in evolutionary units for an unrooted tree topology with no fossil calibrations. For the unrooted tree, we use the same tree as in the node age simulations in unrooted format. We also conduct simulations in which the $GTR + \Gamma$ substitution model parameters are estimated from the simulated data, rather than fixed to the true values. These simulations settings are described in the Appendix.

3.3 Bird divergence analysis

We apply the pairwise likelihood to a node dating analysis using the bird genome alignment data of Wu et al. (2024a). The data consist of 100 clock-like protein coding genes. These genes are subsampled from the 1000 genes with the least degree of molecular clock violation collected from a whole genome analysis by Wu et al. (2024a). Wu et al. (2024a) collected genomic data from 125 taxa, including 118 modern bird *Neoaves* and an outgroup of 6 ancient birds *Paleoaves*, and the American alligator. We use

a)



b)

Calibration Setting	Setting ID	Fossil	Node ID	True Node Age	Prior Calibration
Correct Calibration	1	1	1	275.3	U(255.9, 299.8)
		2	2	84.5	OLN(66.7, 81.3, 5.3)
		3	5	59.0	OE(51.6, 72.8)
		4	9	46.27	OE(28.3, 61.2)
Prior Misspecified	2	3	5	59.0	OE(61.6, 72.8)
	3	2	2	84.5	OLN(66.7, 82.6, 9.2)
	4	2	2	84.5	OLN(66.7, 89.3, 31.8)
Fossil Misplaced	5	3	6	32.8	OE(51.6, 72.8)
	6	3	4	67.2	OE(51.6, 72.8)
	7	3	3	75.8	OE(51.6, 72.8)

Figure 1: a) 15-taxon tree topology with node ages used for simulations. The Node ID labels are in black text, the Fossils are labeled with red circles, and the node ages are in blue text.

b) Summary of fossil calibration settings used for node age estimation simulations. In Setting 1, the fossils are placed correctly and the node ages are calibrated using prior distributions that are correct for the true node ages. In Settings 2-4, the prior distributions are changed, and in Settings 5-7, Fossil 3 is placed on a different node. For Settings 2-7, the change from the correct fossil setting or prior distribution is indicated.

20 fossils to calibrate the clock model; these fossils are the same as in Wu et al. (2024b). For the split between *Neognathae* and *Paleognathae* (Paleo-Neogene), we consider three different node age calibrations based on the calibrations used by Wu et al. (2024a). They use lower and upper bounds in MCMCTree with a soft upper ‘bound’ that allows the MCMC samples to violate the upper bound with probability 0.025 (Yang, 2007). We use lognormal distributions shifted to have the same lower bound and with 0.025 of the distribution mass above the soft upper ‘bound’. The full fossil calibration details are in the Supplementary Materials. In order to compare the results of the node age estimation using the pairwise likelihood, we assume the same tree topology estimated in Wu et al. (2024a) (Figure 7)

For the full likelihood model, parameters are sampled from MCMC chains of 2,000,000 generations, thinned by retaining every 500th sample, and the first 50% of samples are discarded as burn-in. The APW1, and APW2 are run for 3,000,000 generations with the same settings otherwise. The PW likelihood is run for 4,000,000 generations, as the chains take longer to converge. Two independent runs are conducted with 4 Metropolis-coupled chains in each run. Convergence is monitored by examining trace plots of sampled log-likelihood values (Figure 11). The chains are run in parallel using OpenMPI version 5.0.3, with a separate process for each of the 8 MCMC chains.

3.3.1 Prior distributions

The prior distributions used for the bird divergence time estimation are as follows. The overall mutation rate is given a normal distribution with a mean of 0.001, standard deviation of 0.01, truncated to be greater than 0. The qossil ages are given Offset Exponential distributions with lower bounds given by the minimum age of the fossil, as described in the Appendix. The means of the OE distributions are set to be at the midpoint of the node lower bound and the soft upper bound of the bird ancestral node, the Paleo-Neogene split. The Paleo-Neogene split is calibrated with an OLN(66.7, 81.3, 5.3) distribution; the mean and standard deviation are chosen such that the 97.5th percentile matches the soft upper bound of 94.1 MYA used in Wu et al. (2024a) and the mean is halfway between the lower bound and soft upper bound. The node ages are given the birth-death process prior distribution as implemented in MrBayes version 3.2.7, with default priors on speciation and extinction rate (Exponential with mean 10 and Uniform on [0,1], respectively). We check that the prior distributions on the node ages are reasonable by running the MCMC chain without data and comparing the resulting 95% intervals with those obtained using MCMCTree and the settings used in Wu et al. (2024a).

3.3.2 Fixing substitution model parameters

For the bird divergence time analysis, we fix the substitution model parameters by using the full likelihood model in a short initial MCMC run. We use the MrBayes ‘propset’ command to increase the frequency of relative rate move proposals to 0.1 and α move proposals to 0.1. The tree topology is fixed and all model parameters and branch lengths are sampled for 50,000 generations in 2 independent runs, with the first 8,000 discarded as burn-in. To ensure reasonable values for the substitution models are estimated, we examine the width of the interval estimates and compare the estimates obtained to the parameter estimates obtained in the complete MCMC run using the Full likelihood.

4 Results

4.1 Simulation Results

Under Calibration Setting 1, where calibrated nodes were correctly positioned and assigned appropriate prior distributions, the four likelihood formulations exhibited distinct performance patterns in estimating node ages (Figure 2). Assessment of confidence interval (CI) coverage rates averaged across internal nodes revealed that the APW2 and APW1 likelihoods achieved the highest overall coverage, both exceeding the nominal 0.95 level (Figure 2a). In contrast, the PW likelihood produced the lowest coverage, declining to approximately 0.925 under the 50,000-site condition, although it remained near or above the nominal threshold for shorter alignments. Square-rooted mean squared error (rMSE) comparisons demonstrated that APW2 consistently yielded the lowest values across all sequence lengths (Figure 2b). The PW likelihood produced the highest rMSE, while APW1 and the Full likelihood displayed comparable performance. Node-specific rMSE analyses focused on Nodes 2–6 and 9–10, representing the oldest non-root nodes (1a) and those most affected by calibration perturbations in simulation settings 2–7. At each of these nodes, APW1 and APW2 achieved the lowest rMSE values (Figure 2c).

Computational time analyses indicated that all four likelihoods required approximately 20 seconds to complete MCMC analyses for 1,000-site alignments (Figure 2d). For PW, APW1, and APW2, runtime remained essentially constant with increasing sequence length. In contrast, the Full likelihood exhibited a pronounced increase in computational demand, requiring 75 seconds at 10,000 sites and 250 seconds at 50,000 sites. Comparable runtime patterns were observed under Calibration Settings 2–7 and are therefore not shown.

In Calibration Settings 2–4, the fossil placements are unchanged, but are calibrated with incorrect or less informative priors (Figure 3). The Full likelihood interval coverage rates (averaged over all internal nodes) are lowest of the four likelihoods in Setting 2 (Figure 3a), in which the prior distribution on the calibration for Node 5 has a lower bound higher than the true node age. The APW2 likelihood CIs have the highest coverage rates for all sequence lengths, and the APW1 intervals have higher coverage rates than the PW likelihood for the 1,000 and 10,000 site settings, and a similar rate for the 50,000 site setting. The coverage rates for Calibration Settings 3 and 4 are similar, and are similar to the results of Calibration Setting 1, as the calibrations are correct for the node ages, but the prior distribution on the age of Node 2 less informative. Again, the PW likelihood has the lowest interval coverage rates, and the APW2 and APW1 coverage rates are highest.

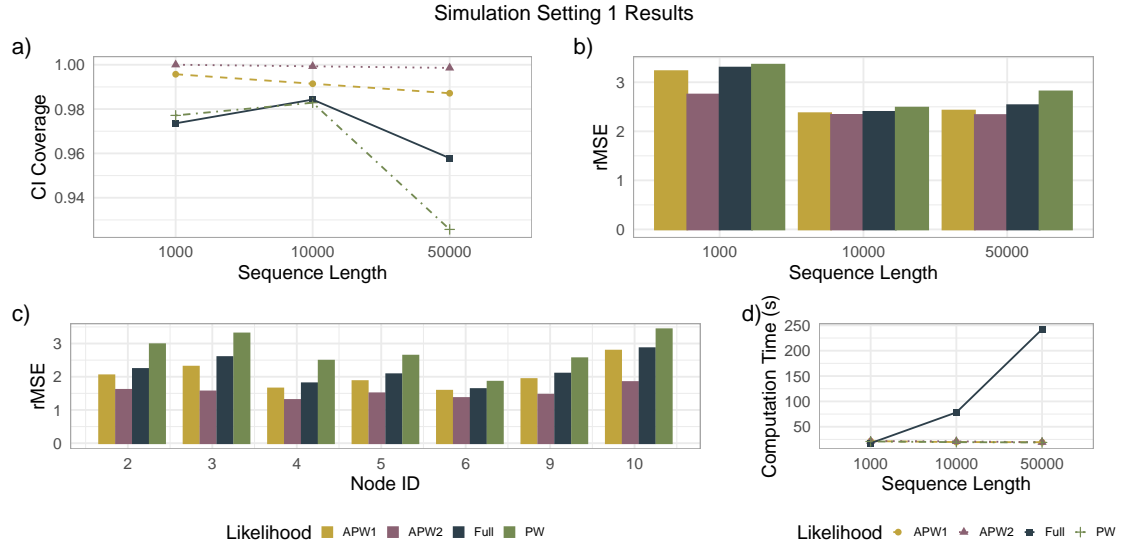


Figure 2: Results of node age simulation Setting 1:

- a) (0.95) Credible Interval coverage rates, averaged across all internal tree nodes;
- b) rMSE, averaged across all internal tree nodes;
- c) rMSE for 50,000 site setting at selected nodes;
- d) Computation time in seconds.

The Full likelihood results are represented by the black bars or black squares connected by solid lines, the PW likelihood results are represented by the green bars or green crosses connected by dot-dashed lines, the APW1 results are represented by the yellow bars or yellow circles connected by dashed lines, and the APW2 results are shown by the maroon bars or maroon triangles connected by dotted lines.

Simulation Settings 2–4 Results

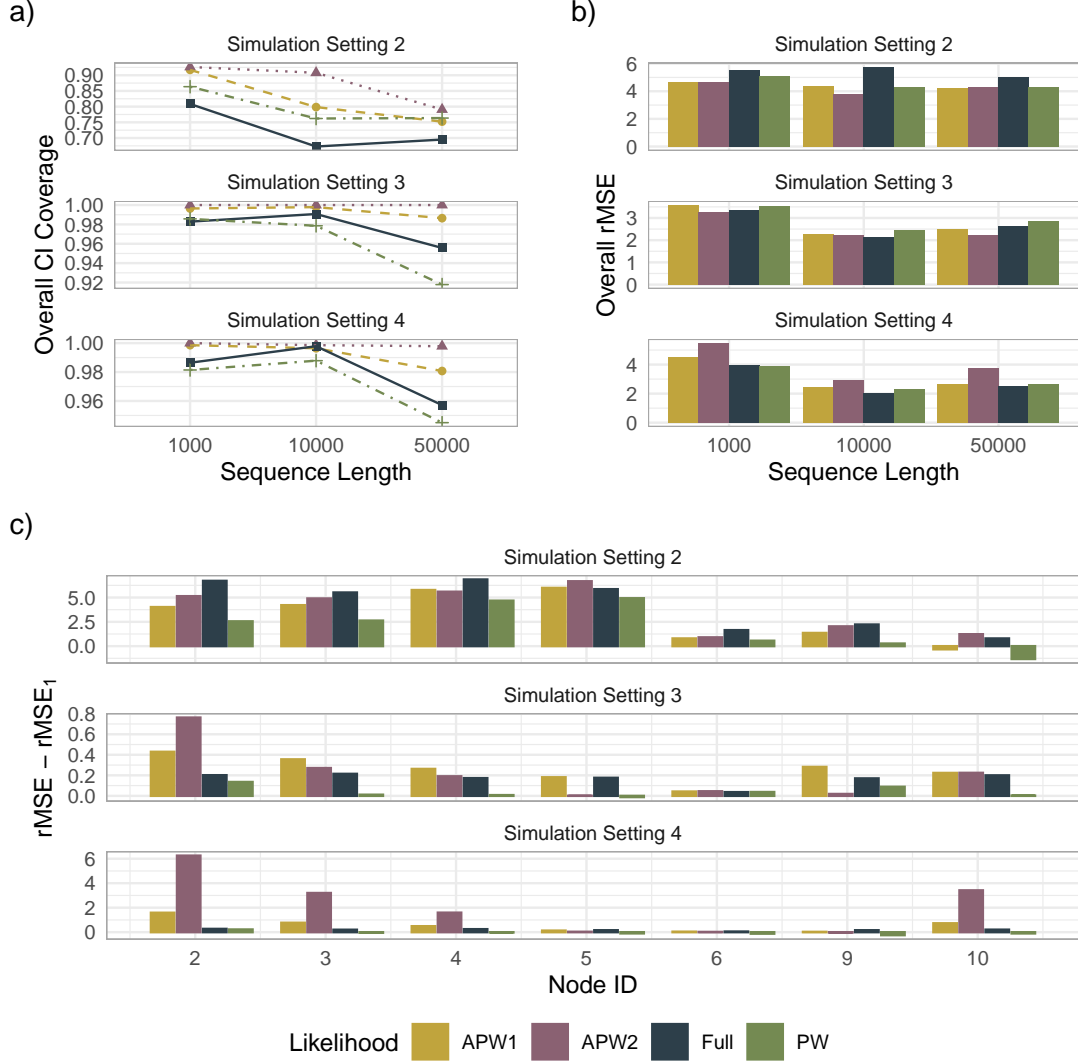


Figure 3: Results of node age simulations where the prior distribution is misspecified, Calibration Settings 2-4.

- a) The CI coverage rates, averaged over all internal nodes;
- b) rMSEs, averaged over all internal nodes;
- c) Difference in rMSEs between Settings 2-4 and Setting 1 for selected internal nodes.

For Calibration Setting 2, the Full likelihood has the highest rMSE overall for all simulated sequence lengths, and although the overall rMSE for the APW2 compares favorably to the Full likelihood in Setting 3, the APW2 likelihood overall rMSE is worst in Setting 4. (Figure 3b). For Settings 2-4, we wish to quantify how the change in fossil calibration affects the node age estimates. We consider the difference between the rMSE obtained in each of Calibration Settings 2-4 and the rMSE in Calibration Setting 1, denoted $rMSE - rMSE_1$. The difference in rMSE represents the change in the quality of the node age estimate caused by the change in node age calibration prior. Unsurprisingly, the quality of estimates for Nodes 2-4 is reduced for all likelihoods in Calibration Setting 2 (Figure 3c); the Full likelihood estimates are the most affected, with the largest change in rMSE at these nodes. The APW1 and APW2 likelihood-based estimates of Node 5 have the largest change in rMSE at that node. The PW likelihood is the least affected, with the least change in rMSE at all nodes. For Calibration Settings 3 and 4, the calibration prior on Node 2 is made less informative. The APW2 based estimates have the

largest increases in rMSE in these settings, with the APW1 likelihoods also showing larger increases in rMSE than the Full likelihood. The interval estimates for all four likelihoods achieve low coverage rates for Nodes 2-4 in Calibration Setting 2, but the Full likelihood intervals have the lowest coverage rates by far, covering the true node ages with a rate of 0 for the 10,000 and 50,000 site settings, the APW1 and APW2 likelihood-based intervals cover these true node ages at much higher rates (Figure 8a). The node-wise changes in rMSE for the 1,000 and 10,000 site settings are similar to those of the 50,000 site setting (Figure 8b).

In Calibration Settings 5-7, the calibration prior distributions are unchanged, but the fossil calibration at Node 5 is misplaced. The fossil is placed at the direct ancestor and descendant nodes, 4 and 6 (Settings 5 and 6, respectively), and then at Node 5's grandparent node, Node 3 (Setting 7). Examining the CI coverage (over all nodes) shows similar coverage rates across the four likelihoods in Calibration Settings 5 and 7, in which the Fossil 3 calibration is placed above the correct node (Figure 4a). The APW2 and APW1 likelihoods achieve the highest coverage rates, and the Full and PW likelihood interval coverage rates are similar. Both Adjusted PW likelihood coverage rates remain above or very near the credible level of 0.95, but both PW and Full likelihood coverage rates drop below the credible level when the number of sites is 50,000; in Calibration Setting 7, both Full and PW likelihood obtain interval coverage rates around 0.825 in the 50,000 site setting. The node age estimates are more affected in Setting 6, in which the lower bound due to Fossil 3 is placed at Node 4, below its correct position. Here, the Full likelihood achieves the lowest CI coverage rate for all sequence lengths. The APW2 likelihood achieves the highest interval coverage rates in the 1000 and 10,000 site settings, and the PW and APW1 likelihoods achieve the highest coverage rates in the 50,000 site setting.

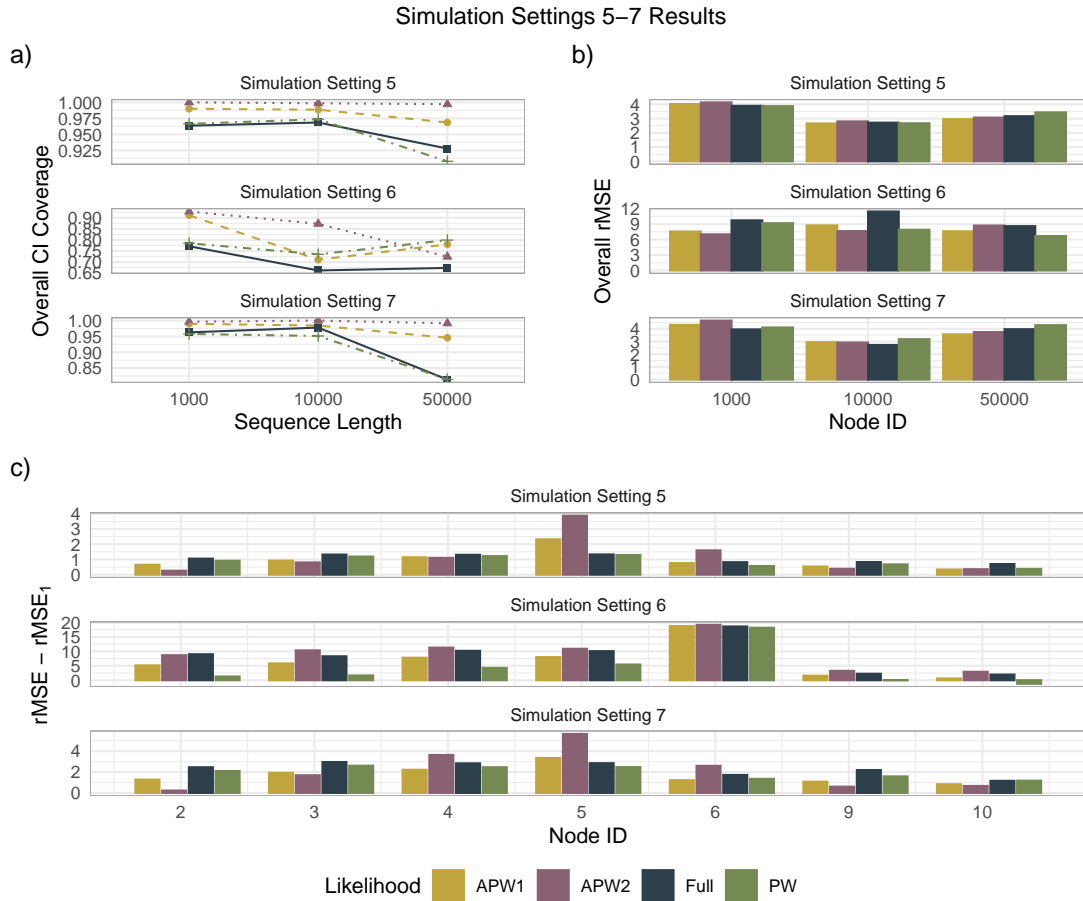


Figure 4: Results of node age simulations in which Fossil 3 is misplaced, Calibration Settings 5-7:

- a) The CI coverage rates, averaged over all internal nodes;
- b) rMSE, averaged over all internal nodes;
- c) Difference in between rMSE in Setting 5-7 and rMSE in Setting 1 for selected internal nodes.

In Calibration Settings 5 and 7, the overall rMSEs are similar; all four likelihoods obtain similar overall rMSEs in the 10,000 site setting, the APW1 and APW2 likelihoods achieve lower rMSEs than the PW and Full likelihoods for 50,000 sites, and for 1,000 sites the PW and Full likelihoods achieve slightly lower rMSEs than the two APW likelihoods. In Setting 6, the Full likelihood overall rMSEs is highest and APW2 is lowest for 1,000 and 10,000 sites, and the APW1 and PW likelihoods achieve lower rMSEs than the Full likelihood for all sequence lengths (Figure 4b). We again compare the node-wise rMSEs to those obtained in Setting 1; the Full likelihood rMSE increases the most at Nodes 2, 3, 9, and 10, the APW1 and APW2 likelihood-based rMSEs increase the most at Node 5, and the APW2 estimates have the largest increase in rMSE at Node 6 (Figure 4c). In Simulation Setting 6, the APW2 and Full likelihood estimates have similar increases in rMSE, with 2-6 being the most affected Nodes. The APW1 likelihood rMSEs increase less than the APW2 and Full likelihoods, and the PW likelihood node age estimates are the least affected by the fossil misplacement, and obtain the lowest overall rMSEs in the 50,000 site settings.

The simulations using the unrooted tree suggest the PW, APW1, and APW2 estimates converge to the true branch lengths as the sequence length increases (Table 2). The supplementary simulations in which the substitution model parameters are estimated from the data indicate there is little effect on the node age estimates if the substitution model parameters are known and fixed or estimated simultaneously (Table 3).

4.2 Bird Divergence Analysis

For the nodes where the fossil calibrations are placed, the interval estimates obtained from the PW likelihood are the narrowest, and the APW1 intervals tend to be narrower than the Full likelihood intervals 5. The APW2 interval estimates are the widest, consistent with the simulation results. The APW2 likelihood results in some point estimates that are much larger than the other likelihoods, for the split between Suboscines and Oscines and the root of Corvidae in the tree in particular; the same is true when considering all estimated node ages (Figure 10). Of interest is whether the radiation of modern bird species began before or after the kPG boundary; we consider nodes whose credible interval is entirely above the kPG boundary 66 MYA. The PW likelihood estimates only 3 such nodes, and the APW1 likelihood estimates 8. The Full and APW2 likelihood estimate 14 and 17, respectively. The estimated substitution model parameters fixed for the PW likelihood analyses are shown in Table 4. A comparison with the estimates from the full run of the node age estimation using the Full likelihood indicates the initial run yields good estimates of the substitution model parameters.

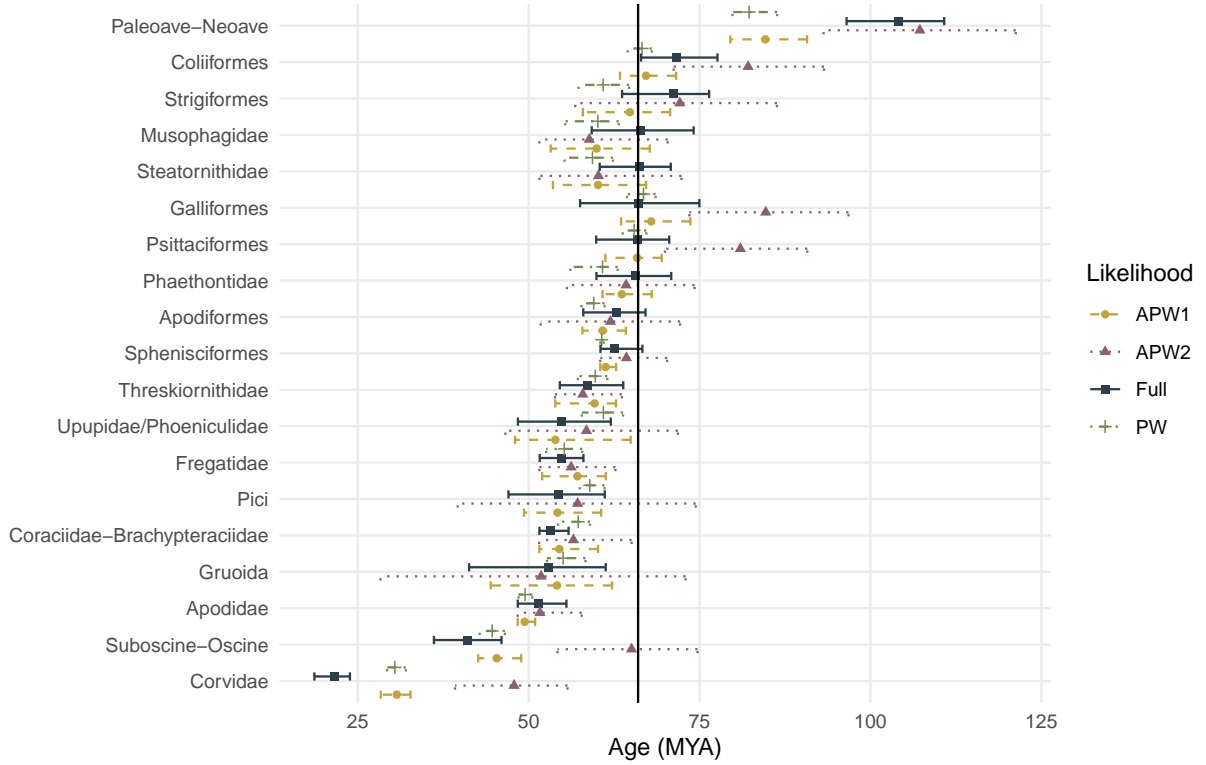


Figure 5: Node age point estimates and credible intervals obtained from the PW (crosses and dotted lines), APW (circles and solid lines), and Full (triangles and dashed lines) likelihoods. The vertical dotted line indicates the kPG boundary, 66 MYA. The nodes on the y-axis are arranged in descending order of the APW point estimate. Note the break in scale on the x-axis, to show the estimates of the root node.

The APW2 likelihood-based estimates have much wider credible intervals than the PW and APW1 likelihoods, indicating more uncertainty in the estimated node ages. For the oldest nodes in the tree, the PW and APW1 likelihoods tend to result in younger estimates than the Full likelihood, as seen in the points near the kPG line falling below the $x = y$ line (Figure 6). This is more pronounced in the PW likelihood estimates, whose interval estimates are also narrower than the APW1 intervals. The APW2 likelihood node age estimates tend to overestimate the node ages in this region of the tree, but the wider CIs reflect more uncertainty in the estimates, and tend to cover the Full likelihood point estimates. For nodes whose estimated age is between 10 MYA and about 50 MYO, all of the PW and APW likelihoods tend to overestimate the node age, relative to the Full likelihood. However, the wider credible intervals resulting from the adjustment weighted likelihoods often cover the estimate from the Full likelihood. Of the 124 internal nodes, the APW2 CI for the node age covers the point estimate from the Full likelihood for 94, and the number of nodes for which the credible intervals obtained from the APW2 and Full likelihoods overlap is 109. The CIs from the APW1 estimates cover the Full likelihood point estimates and CIs for 81 and 111 nodes, and the CIs obtained from the PW likelihood overlap the Full likelihood point estimate and intervals for 39 and 91, respectively.

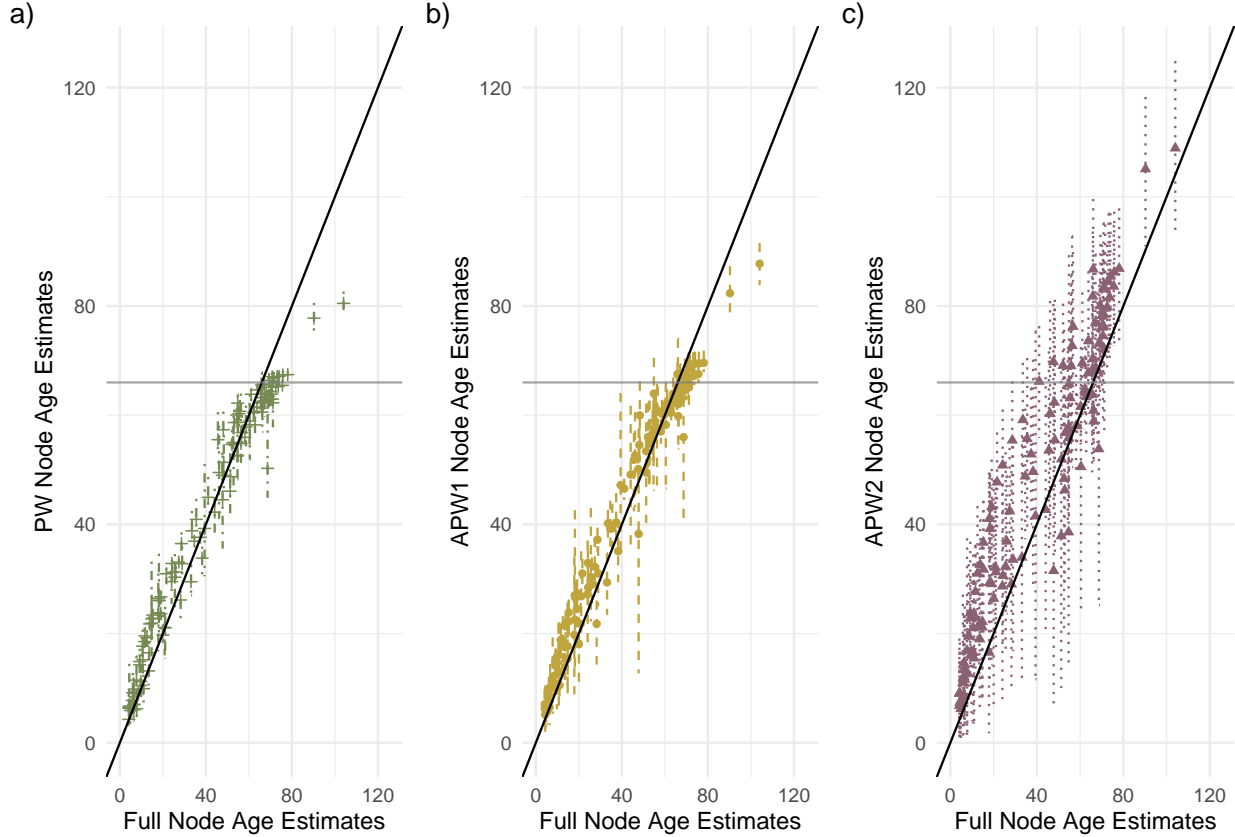


Figure 6: a) Node age estimates obtained from PW and Full likelihood.
b) Node age estimates obtained from APW1 and Full likelihoods.
c) Node age estimates obtained from APW2 and Full likelihoods.
The horizontal gray line indicates the kPG boundary, and the black line is the $x = y$ line. The dot-dashed, dashed, and dotted lines show the PW, APW1, and APW2 credible intervals.

The MCMC running times for the bird divergence time analysis are given in Table 1. The PW and Adjusted PW likelihoods enjoy a considerable computational advantage over the Full likelihood; with computation times between 119 and 167 minutes, the PW models are on average 27 times faster than the Full likelihood models, which take between 3412 and 4043 minutes to complete. The initial run used to estimate the substitution model parameters uses 246 minutes; even accounting for this, and the longer MCMC chains, the total running times for the PW and APW likelihoods are substantially faster than the Full likelihood.

Likelihood	MCMC Run Time (Minutes)		
	Main Run	Initial Run	Total
PW	278.0	240.2	518.2
APW1	163.4	240.2	403.6
APW2	245.8	240.2	486.0
Full	6204.0	NA	6204.0

Table 1: Computation times for bird divergence time analysis. The initial run is used to estimate the substitution model parameters, which are fixed in the PW and APW runs. For the PW likelihood, the main run takes longer to converge, using 4,000,000 generations

In the bird alignment data example, our results using the APW2 likelihood are similar to the results of Wu et al. (2024a), which is not unexpected since we use the same fossil calibrations and attempt

to calibrate the priors to mimic the use of MCMCTree with soft constraints. It is known that different software packages construct the node age prior differently given the same fossil calibrations, which affects node dating results (Barba-Montoya et al., 2017). However, the results of our analysis with the APW2 and Full likelihoods arrive at similar conclusions that the radiation of modern birds began before the kPG boundary. Our node age estimates from both the APW2 and Full likelihood are somewhat younger than theirs, however. The results of the APW1 and APW2 estimates differ somewhat; although in the simulations the APW1 behaves similarly to the Full likelihood, in the bird data analysis, the APW2 has better agreement with the Full likelihood, and the APW1 and PW likelihood based results are more similar, and favor more recent divergences. Although the simulation results indicate both adjustment weights work well if the prior and data agree, the APW2 leads to wider credible intervals and greater uncertainty in the posterior estimates, particularly for younger nodes. However, the simulations indicate that the credible intervals (of all four likelihoods) fail to adequately reflect the uncertainty in the estimated fossil ages in many cases. Ultimately, accuracy of the fossil calibrations is certainly the most critical element in obtaining accurate estimates from the posterior distribution of node ages, despite the choice of likelihood used.

5 Discussion

Accurate estimation of node ages from phylogenomic data remains a considerable challenge. The pairwise likelihood (PW) and its adjusted variants (APW1 and APW2) offer substantial computational advantages over the full-likelihood approach because their complexity is independent of sequence length. For example, in the avian dataset, the primary MCMC analysis using PW and APW was approximately 25 times faster than the full-likelihood method, with similar gains observed in simulation studies. This advantage becomes increasingly pronounced for longer sequences, making APW particularly advantageous when analyzing concatenated alignments. Beyond computational efficiency, our simulations reveal a fundamental trade-off between estimation precision and methodological robustness. The full-likelihood approach produced the most accurate point estimates of node ages; however, this precision was accompanied by pronounced sensitivity to prior misspecification, leading to substantial performance degradation under scenarios involving fossil calibration errors. In contrast, PW demonstrated strong robustness to such inaccuracies, albeit at the cost of reduced precision. The adjusted pairwise likelihoods (APW1 and APW2) effectively reconciled these competing properties. By retaining the accuracy of the full-likelihood method while incorporating the robustness of PW, the adjusted approaches achieved a balance between precision and stability. Consequently, APW1 and APW2 consistently outperformed both original methods, providing the most reliable interval coverage of true node ages across all simulation conditions.

Genomic-scale phylogenetic datasets are often comprised of data from many genes, and it is perhaps not realistic to assume a single substitution process is shared across all possible model partitions. On the other hand, models with many partitions require many parameters, which can render model estimation and MCMC convergence problematic. Under-partitioned models can perform capably for node age estimation if the prior distributions and the clock model are not badly violated (Angelis et al., 2017). In the case of genomic data, many loci may have significant congruence, and concatenating loci into longer sequences can provide a simpler modeling framework (Leigh et al., 2008). The use of the pairwise likelihood then seems reasonable in settings when the data can be grouped into a few similar, long partitions. Use of a variable site-rate model like the GTR+ Γ can compensate somewhat for differing substitution processes at different sites and realistic, highly parameterized models that fit different substitution processes often have difficulty converging.

The most difficult aspect of the pairwise likelihood is computing the adjustment weight. We focus on two of the most simple proposed weights, and we estimate them only via estimates of the matrices J and H obtained by taking subsets of the existing alignment. In the case of the simulated data, these data subsets are clearly appropriate, as the model from which the data are simulated is known; in the case of real data however, the assumption of independent and identical data partitions may not be met. In our observation, the APW2 adjustment weight is a smaller constant than the APW1 weight, which has the effect of flattening the APW2 posterior distribution, and can result in too-wide credible intervals, as seen in the simulation CI coverage rates above the credible level. The adjustment weights are possibly more problematic to compute in this case than in other applications of the composite likelihood, as the weight estimate is of much higher dimension than in typical applications (Varin et al., 2011; Ribatet et al., 2012; Cattelan and Varin, 2013; Cattelan and Sartori, 2015). Using simulated sequences to approximate the weight as in Cattelan and Varin (2013) may provide more robust estimates of the adjustment weights, and using lower dimensional approximations to the H and J matrix or approaches based on down-weighting

less informative taxa pairs as in Holder and Steel (2011) may be an interesting approach. To simplify the adjustment weight computation, we assume fixed parameters for the *GTR* substitution model.

Our simulations show the pairwise likelihood can be used for fast and accurate node age estimation, under different substitution model settings and settings where fossil calibrations provide inaccurate prior information. However, our study focuses on a single relaxed clock model and a single 15-taxa tree topology. More extensive simulation using more varied tree topologies, clock model or substitution model parameter settings could be undertaken to examine the behavior of the PW and APW likelihoods in realistic scenarios. Further work could use examine the performance of node age estimation when other aspects of the model like the clock model form are misspecified, or make use of a Bayes factor Kass (1995) based on the APW likelihood to apply the APW to model selection.

Node dating is a challenging problem in phylogenetic analysis. Increasing availability of genomic data poses a challenge, as likelihood based statistical methods can be computationally prohibitive for large datasets. We employ the pairwise composite likelihood in a Bayesian model to address this problem for long sequences; since computation of the pairwise composite likelihood doesn't scale with sequence length, it can be applied to large sequence alignments when the full likelihood would be infeasible. We propose adjusting the pairwise likelihood with an adjustment weight derived from the asymptotic form of the composite LRT; our simulation results indicate this adjustment compensates for the simplifying assumptions of the composite likelihood, and results in posterior interval estimates that better reflect the uncertainty in the estimated node ages. Additionally, our simulation results suggest the pairwise likelihood is robust to fossil miscalibrations when estimating long-ago divergence times, an intriguing feature as there is considerable uncertainty and disagreement in the placement of fossils.

6 Software and Data Availability

The pairwise likelihood is implemented as a source Bayesian phylogenetic software **MrBayes** version 3.2.7. The implementation is designed not to interfere with the other features of MrBayes, so the pairwise likelihood and adjustment weights are available to use with a wide variety of existing phylogenetic models. As of now, the pairwise likelihood is available only for DNA type data, and the GTR and JC substitution models. The PW and APW likelihoods are implemented to work with existing MrBayes functionality, including MPI parallelization, model partitioning, and stepping-stone sampling (Xie et al., 2010). The source code is available for compilation from <https://www.github.com/gmellison/PwBayes>, which also includes scripts used for the simulations. No new data were used for this study. Bird genomic were previously made available at <https://doi.org/10.6084/m9.figshare.21499230.v1> (Liu and Wu, 2024) and <https://doi.org/10.26036/cnp0002307> (Qu, 2024).

7 Acknowledgments

We would like to thank the authors of (Wu et al., 2024a) for helpful discussion and for providing their tree topology and sequence data. This study was supported in part by resources and technical expertise from the Georgia Advanced Computing Resource Center.

References

- Konstantinos Angelis, Sandra Álvarez Carretero, Mario Dos Reis, and Ziheng Yang. An evaluation of different partitioning strategies for bayesian estimation of species divergence times. *Systematic Biology*, 67(1):61–77, July 2017. ISSN 1076-836X. doi: 10.1093/sysbio/syx061.
- Jose Barba-Montoya, Mario Dos Reis, and Ziheng Yang. Comparison of different strategies for using fossil calibrations to generate the time prior in bayesian molecular clock dating. *Molecular Phylogenetics and Evolution*, 114:386–400, September 2017. ISSN 1055-7903. doi: 10.1016/j.ympev.2017.07.005.
- MJ Benton, PCJ Donoghue, and RJ Asher. *Calibrating and constraining molecular clocks*, pages 35 – 86. Oxford University Press, United Kingdom, 2009. ISBN 0199535035.
- Estelle Bourdon, Baâdi Bouya, and Mohamed Iarochene. Earliest african neornithine bird: A new species of prophaethontidae (aves) from the paleocene of morocco. *Journal of Vertebrate Paleontology*, 25(1): 157–170, 3 2005. doi: 10.1671/0272-4634(2005)025[0157:eanban]2.0.co;2.

- Pierce Brodkorb. Neogene fossil jays from the great plains. *Condor*, 74:347–349, 1972.
- M. Cattelan and N. Sartori. Empirical and simulated adjustments of composite likelihood ratio statistics. *Journal of Statistical Computation and Simulation*, 86(5):1056–1067, June 2015. ISSN 1563-5163. doi: 10.1080/00949655.2015.1053091.
- Manuela Cattelan and Cristiano Varin. Hybrid pairwise likelihood analysis of animal behavior experiments. *Biometrics*, 69(4):1002–1011, September 2013. ISSN 1541-0420. doi: 10.1111/biom.12090.
- R. E. Chandler and S. Bate. Inference for clustered data using the independence loglikelihood. *Biometrika*, 94(1):167–183, February 2007. ISSN 1464-3510. doi: 10.1093/biomet/asm015.
- Santiago Claramunt, Edward L. Braun, Joel Cracraft, Jon Fjeldså, Simon Y. W. Ho, Peter Houde, Jacqueline M. T. Nguyen, and Josefin Stiller. Calibrating the genomic clock of modern birds using fossils. *Proceedings of the National Academy of Sciences*, 121(39), September 2024. ISSN 1091-6490. doi: 10.1073/pnas.2405887121.
- Julia Clarke, Daniel Ksepka, N Smith, and Mark Norell. Combined phylogenetic analysis of a new north american fossil species confirms widespread eocene distribution for stem rollers (aves, coracii). *Zoological Journal of the Linnean Society*, 157(3):586–611, 10 2009. doi: 10.1111/j.1096-3642.2009.00550.x.
- Mario Dos Reis and Ziheng Yang. The unbearable uncertainty of bayesian divergence time estimation. *Journal of Systematics and Evolution*, 51(1):30–43, December 2012. ISSN 1759-6831. doi: 10.1111/j.1759-6831.2012.00236.x.
- Alexei J Drummond, Simon Y. W Ho, Matthew J Phillips, and Andrew Rambaut. Relaxed phylogenetics and dating with confidence. *Plos Biology*, 4(5):e88, March 2006. ISSN 1545-7885. doi: 10.1371/journal.pbio.0040088.
- Gareth J. Dyke and Joanne H. Cooper. A new psittaciform bird from the london clay (lower eocene) of england. *Palaeontology*, 43(2):271–285, June 2000. ISSN 1475-4983. doi: 10.1111/1475-4983.00126.
- James S. Farris. Distance Data Revisited. *Cladistics*, 1(1):67–86, 1985. ISSN 1096-0031. doi: 10.1111/j.1096-0031.1985.tb00411.x.
- Daniel Field and Allison Hsiang. Nearctic origins of the 'endemic' african avifauna? the necessity of fossils for avian historical biogeography. *Journal of Vertebrate Paleontology*, page 129, 2014. ISSN 1937-2809.
- Daniel J. Field, Michael Hanson, David Burnham, Laura E. Wilson, Kristopher Super, Dana Ehret, Jun A. Ebersole, and Bhart-Anjan S. Bhullar. Complete ichthyornis skull illuminates mosaic assembly of the avian head. *Nature*, 557(7703):96–100, May 2018. ISSN 1476-4687. doi: <https://doi.org/10.1038/s41586-018-0053-y>.
- Daniel J. Field, Juan Benito, Albert Chen, John W. M. Jagt, and Daniel T. Ksepka. Late cretaceous neornithine from europe illuminates the origins of crown birds. *Nature*, 579(7799):397–401, March 2020. ISSN 1476-4687. doi: <https://doi.org/10.1038/s41586-020-2096-0>.
- Félix Forest. Calibrating the tree of life: Fossils, molecules and evolutionary timescales. *Annals of Botany*, 104(5):789–794, August 2009. ISSN 0305-7364. doi: 10.1093/aob/mcp192.
- Helena Geys, Geert Molenberghs, and Louise M. Ryan. Pseudolikelihood modeling of multivariate outcomes in developmental toxicology. *Journal of the American Statistical Association*, 94(447):734–745, September 1999. ISSN 1537-274X. doi: 10.2307/2669986.
- Shannon J. Hackett, Rebecca T. Kimball, Sushma Reddy, Rauri C. K. Bowie, Edward L. Braun, Michael J. Braun, Jena L. Chojnowski, W. Andrew Cox, Kin-Lan Han, John Harshman, Christopher J. Huddleston, Ben D. Marks, Kathleen J. Miglia, William S. Moore, Frederick H. Sheldon, David W. Steadman, Christopher C. Witt, and Tamaki Yuri. A phylogenomic study of birds reveals their evolutionary history. *Science*, 320(5884):1763–1768, June 2008. ISSN 1095-9203. doi: 10.1126/science.1157704.

- Colin J. O. Harrison. A revision of the fossil swifts (vertebrata, aves, suborder apodi), with descriptions of three new genera and two new species. *Mededelingen van de Werkgroep voor Tertiaire en Kwartaire Geologie*, 21:157–177, 1984.
- Michael Heads. Dating nodes on molecular phylogenies: A critique of molecular biogeography. *Cladistics*, 21(1):62–78, February 2005. ISSN 1096-0031. doi: 10.1111/j.1096-0031.2005.00052.x.
- Mark T. Holder and Mike Steel. Estimating phylogenetic trees from pairwise likelihoods and posterior probabilities of substitution counts. *Journal of Theoretical Biology*, 280(1):159–166, July 2011. ISSN 0022-5193. doi: 10.1016/j.jtbi.2011.04.005.
- Peter Houde and Storrs L. Olson. A radiation of coly-like birds from the eocene of north america (aves: Sandcoleiformes new order). In K. Campbell, editor, *Papers in Avian Paleontology Honoring Pierce Brodkorb*, volume 36, pages 137–160. Natural History Museum of Los Angeles County Science Series, 1992.
- Laura A. Hug and Andrew J. Roger. The impact of fossils and taxon sampling on ancient molecular dating analyses. *Molecular Biology and Evolution*, 24(8):1889–1897, June 2007. ISSN 0737-4038. doi: 10.1093/molbev/msm115.
- Jun Inoue, Philip C. J. Donoghue, and Ziheng Yang. The impact of the representation of fossil calibrations on bayesian estimation of species divergence times. *Systematic Biology*, 59(1):74–89, November 2009. ISSN 1063-5157. doi: 10.1093/sysbio/syp078.
- Erich D. Jarvis, Siavash Mirarab, Andre J. Aberer, Bo Li, Peter Houde, Cai Li, Simon Y. W. Ho, Brant C. Faircloth, Benoit Nabholz, Jason T. Howard, Alexander Suh, Claudia C. Weber, Rute R. Da Fonseca, Jianwen Li, Fang Zhang, Hui Li, Long Zhou, Nitish Narula, Liang Liu, Ganesh Ganapathy, Bastien Boussau, Md. Shamsuzzoha Bayzid, Volodymyr Zavidovych, Sankar Subramanian, Toni Gabaldón, Salvador Capella-Gutiérrez, Jaime Huerta-Cepas, Bhanu Rekepalli, Kasper Munch, Mikkel Schierup, Bent Lindow, Wesley C. Warren, David Ray, Richard E. Green, Michael W. Bruford, Xiangjiang Zhan, Andrew Dixon, Shengbin Li, Ning Li, Yinhua Huang, Elizabeth P. Derryberry, Mads Frost Bertelsen, Frederick H. Sheldon, Robb T. Brumfield, Claudio V. Mello, Peter V. Lovell, Morgan Wirthlin, Maria Paula Cruz Schneider, Francisco Prosdoci, José Alfredo Samaniego, Amhed Missael Vargas Velazquez, Alonzo Alfaro-Núñez, Paula F. Campos, Bent Petersen, Thomas Sicheritz-Ponten, an Pas, Tom Bailey, Paul Scofield, Michael Bunce, David M. Lambert, Qi Zhou, Polina Perelman, Amy C. Driskell, Beth Shapiro, Zijun Xiong, Yongli Zeng, Shiping Liu, Zhenyu Li, Binghang Liu, Kui Wu, Jin Xiao, Xiong Yinqi, Qiuemei Zheng, Yong Zhang, Huanming Yang, Jian Wang, Linnea Smeds, Frank E. Rheindt, Michael Braun, Jon Fjeldsa, Ludovic Orlando, F. Keith Barker, Knud Andreas Jönsson, Warren Johnson, Klaus-Peter Koepfli, Stephen O’Brien, David Haussler, Oliver A. Ryder, Carsten Rahbek, Eske Willerslev, Gary R. Graves, Travis C. Glenn, John McCormack, Dave Burt, Hans Ellegren, Per Alström, Scott V. Edwards, Alexandros Stamatakis, David P. Mindell, Joel Cracraft, Edward L. Braun, Tandy Warnow, Wang Jun, M. Thomas P. Gilbert, and Guojie Zhang. Whole-genome analyses resolve early branches in the tree of life of modern birds. *Science*, 346(6215):1320–1331, 2014. doi: 10.1126/science.1253451.
- Thomas H. Jukes and Charles R. Cantor. Evolution of protein molecules. *Mammalian Protein Metabolism*, 3(24):21–132, 1969. URL <https://books.google.com/books?hl=en&lr=&id=FDHLBAAQBAJ&oi=fnd&pg=PA21&ots=bncpVLWZoy&sig=dWIB5mYAM-4XR5UY>
- Adrian Kass, Robert & Raftery. Bayes Factors. *Journal of the American Statistical Association*, 90(430):773–795, June 1995. ISSN 0162-1459, 1537-274X. doi: 10.2307/2291091. URL <https://www.webofscience.com/api/gateway?GWVersion=2&SrcAuth=D0ISource&SrcApp=WOS&KeyAID=10.2307/2291091&De> Web of Science ID: WOS:A1995RA10400045.
- Sungsik Kong, David L Swofford, and Laura S Kubatko. Inference of phylogenetic networks from sequence data using composite likelihood. *Systematic Biology*, 74(1):53–69, October 2024. ISSN 1076-836X. doi: 10.1093/sysbio/syae054.
- D. T. Ksepka, J. A. Clarke, S. Nesbitt, F. Kulp, and L. Grande. Fossil evidence of wing shape in a stem relative of swifts and hummingbirds (aves, pan-apodiformes). *Proceedings of the Royal Society B*, 280(20130580):1–9, 2013.

- Daniel T. Ksepka. Broken gears in the avian molecular clock: new phylogenetic analyses support stem galliform status for gallinuloides wyomingensis and rallid affinities for amittabha urbsinterdictensis. *Cladistics*, 25(2):173–197, April 2009. ISSN 1096-0031. doi: <https://doi.org/10.1111/j.1096-0031.2009.00250.x>.
- Daniel T. Ksepka and Julia A. Clarke. Primobucco mcgrewi (aves: Coracii) from the eocene green river formation: new anatomical data from the earliest constrained record of stem rollers. *Journal of Vertebrate Paleontology*, 30(1):215–225, January 2010. ISSN 1937-2809. doi: 10.1080/02724630903412414.
- Sudhir Kumar, Michael Suleski, Jack M Craig, Adrienne E Kasprowicz, Maxwell Sanderford, Michael Li, Glen Stecher, and S Blair Hedges. Timetree 5: An expanded resource for species divergence times. *Molecular Biology and Evolution*, 39(8), August 2022. ISSN 1537-1719. doi: <https://doi.org/10.1093/molbev/msac174>.
- Jessica W. Leigh, Edward Susko, Manuela Baumgartner, and Andrew J. Roger. Testing congruence in phylogenomic analysis. *Systematic Biology*, 57(1):104–115, February 2008. ISSN 1063-5157. doi: <https://doi.org/10.1080/10635150801910436>.
- Thomas Lepage, David Bryant, Hervé Philippe, and Nicolas Lartillot. A General Comparison of Relaxed Molecular Clock Models. *Molecular Biology and Evolution*, 24(12):2669–2680, December 2007. ISSN 0737-4038. doi: 10.1093/molbev/msm193.
- Bruce G. Lindsay. Composite likelihood methods. *Statistical Inference from Stochastic Processes*, pages 221–239, 1988. ISSN 0271-4132. doi: 10.1090/conm/080/999014.
- Liang Liu and Shaoyuan Wu. Genomes, fossils and the concurrent rise of modern birds and angiosperms in late cretaceous. 2024. doi: <https://doi.org/10.6084/m9.figshare.21499230.v1>.
- Liang Liu, Lili Yu, and Scott V Edwards. A maximum pseudo-likelihood approach for estimating species trees under the coalescent model. *Bmc Evolutionary Biology*, 10(1):1–18, 2010.
- Liang Liu, Zhenxiang Xi, Shaoyuan Wu, Charles C Davis, and Scott V Edwards. Estimating phylogenetic trees from genome-scale data. *Annals of the New York Academy of Sciences*, 1360(1):36–53, 2015.
- Arong Luo, David a Duchêne, Chi Zhang, Chao-Dong Zhu, and Simon Y W Ho. A simulation-based evaluation of tip-dating under the fossilized birth–death process. *Systematic Biology*, 69(2):325–344, May 2019. ISSN 1076-836X. doi: 10.1093/sysbio/syz038.
- G. Mayr. An owl from the paleocene of walbeck, germany. *Fossil Record*, 5(1):283–288, January 2002. ISSN 2193-0074. doi: 10.1002/mmng.20020050117.
- Gerald Mayr. Tiny hoopoe-like birds from the middle eocene of messel (germany). *The Auk*, 117:968–974, 2000.
- Gerald Mayr. Phylogeny of early tertiary swifts and hummingbirds (aves: Apodiformes). *The Auk*, 120:145–151, 2003.
- Gerald Mayr. A tiny barbet-like bird from the lower oligocene of germany: the smallest species and earliest substantial fossil record of the pici (woodpeckers and allies). *The Auk*, 122:1055–1063, 2005.
- Gerald Mayr. First fossil skull of a paleogene representative of the pici (woodpeckers and allies) and its evolutionary implications. *Ibis*, 148:824–827, 2006a.
- Gerald Mayr. New specimens of the eocene messelirrisoridae (aves: Bucerotes), with comments on the preservation of uropygial gland waxes in fossil birds from messel and the phylogenetic affinities of bucerotes. *Paleontologische Zeitschrift*, 80:405–420, 2006b.
- Gerald Mayr and Sara Bertelli. A record of rhynchaetidae (aves, threskiornithidae) from the early eocene fur formation of denmark, and the affinities of the alleged parrot mopsitta. *Palaeobiodiversity and Palaeoenvironments*, 91(3):229–236, 4 2011. doi: 10.1007/s12549-011-0050-8.
- Jeffrey W. Miller. Asymptotic Normality, Concentration, and Coverage of Generalized Posteriors. *Journal of Machine Learning Research*, 22, 2021. ISSN 1532-4435. URL <https://www.webofscience.com/wos/woscc/full-record/WOS:000687124900001>. Web of Science ID: WOS:000687124900001.

- Alphonse Milne-Edwards. *Recherches Anatomiques et Paléontologiques pour Servir à l'Histoire des Oiseaux Fossiles de la France*. Masson, Paris, 1867-1871.
- Jiří Mlíkovský. *Cenozoic birds of the World. Part 1: Europe*. NINOX Press, Praha, 2002.
- C. Mourer-Chauviré. A large owl from the palaeocene of france. *Palaeontology*, 37:339–348, 1994.
- Laura P. A. Mulvey, Mark C. Nikolic, Bethany J. Allen, Tracy A. Heath, and Rachel C. M. Warnock. From fossils to phylogenies: Exploring the integration of paleontological data into bayesian phylogenetic inference. *Paleobiology*, 51(1):214–236, February 2025. ISSN 1938-5331. doi: 10.1017/pab.2024.47.
- Fábrica F. Nascimento, Mario Dos Reis, and Ziheng Yang. A biologist’s guide to bayesian phylogenetic analysis. *Nature Ecology & Evolution*, 1(10):1446–1454, September 2017. ISSN 2397-334X. doi: 10.1038/s41559-017-0280-x.
- Sterling J. Nesbitt, Daniel T. Ksepka, and Julia A. Clarke. Podargiform affinities of the enigmatic fluviaviridavis platyrhamphus and the early diversification of strisores (“caprimulgiformes” + apodiformes). *PLoS ONE*, 6(11):e26350, November 2011. ISSN 1932-6203. doi: 10.1371/journal.pone.0026350.
- Jacqueline M. T. Nguyen and Simon Y. W. Ho. Calibrations from the fossil record. pages 117–133, 2020. doi: 10.1007/978-3-030-60181-2.8.
- S Olson. volume 36 of *Natural History Museum of Los Angeles County Science Series*, pages 137–160. Los Angeles, Calif, 1992.
- Storrs Olson. A lower eocene frigatebird from the green river formation of wyoming (pelecaniformes: Fregatidae). *Smithsonian Contributions to Paleobiology*, (35):1–33, 1977. doi: 10.5479/si.00810266.35.1.
- Storrs L. Olson. An early eocene oilbird from the green river formation of wyoming (caprimulgiformes: Steatornithidae). *Documents des Laboratoires de Géologie de Lyon*, (99):57–69, 1987.
- James F. Parham, Philip C. J. Donoghue, Christopher J. Bell, Tyler D. Calway, Jason J. Head, Patricia A. Holroyd, Jun G. Inoue, Randall B. Irmis, Walter G. Joyce, Daniel T. Ksepka, José S. L. Patané, Nathan D. Smith, James E. Tarver, Marcel Van Tuinen, Ziheng Yang, Kenneth D. Angielczyk, Jenny M. Greenwood, Christy A. Hipsley, Louis Jacobs, Peter J. Makovicky, Johannes Müller, Krister T. Smith, Jessica M. Theodor, Rachel C. M. Warnock, and Michael J. Benton. Best practices for justifying fossil calibrations. *Systematic Biology*, 61(2):346–359, September 2011. ISSN 1063-5157. doi: 10.1093/sysbio/syr107.
- José S. L. Patané, Joaquim Martins, and João C. Setubal. Phylogenomics. pages 103–187, December 2017. ISSN 1940-6029. doi: 10.1007/978-1-4939-7463-4.5.
- Francesco Pauli, Walter Racugno, and Laura Ventura. Bayesian composite marginal likelihoods. *Statistica Sinica*, 21(1):149–164, 2011. ISSN 10170405, 19968507. URL <http://www.jstor.org/stable/24309266>.
- Jing Peng, David L Swofford, and Laura Kubatko. Estimation of speciation times under the multispecies coalescent. *Bioinformatics*, 38(23):5182–5190, October 2022. ISSN 1367-4811. doi: 10.1093/bioinformatics/btac679.
- Richard O. Prum, Jacob S. Berv, Alex Dornburg, Daniel J. Field, Jeffrey P. Townsend, Emily Moriarty Lemmon, and Alan R. Lemmon. A comprehensive phylogeny of birds (aves) using targeted next-generation dna sequencing. *Nature*, 526(7574):569–573, October 2015. ISSN 1476-4687. doi: 10.1038/nature15697.
- Yanhua Qu. The genome of *Prunella strophiatea*. 2024. doi: 10.26036/CNP0002307.
- Andrew Rambaut and Nicholas C Grass. Seq-gen: An application for the monte carlo simulation of dna sequence evolution along phylogenetic trees. *Bioinformatics*, 13(3):235–238, 1997.
- Bruce Rannala and Ziheng Yang. Inferring speciation times under an episodic molecular clock. *Systematic Biology*, 56(3):453–466, June 2007. ISSN 1076-836X. doi: <https://doi.org/10.1080/10635150701420643>.

- M. D. Reis and Z. Yang. Approximate likelihood calculation on a phylogeny for bayesian estimation of divergence times. *Molecular Biology and Evolution*, 28(7):2161–2172, February 2011. ISSN 1537-1719. doi: 10.1093/molbev/msr045.
- Mathieu Ribatet, Daniel Cooley, and Anthony C. Davison. Bayesian inference from composite likelihoods, with an application to spatial extremes. *Statistica Sinica*, 22(2):813–845, 2012. ISSN 10170405, 19968507. URL <http://www.jstor.org/stable/24310036>.
- P. V. Rich and D. Bohaska. The world’s oldest owl: A new strigiform from the paleocene of southwestern colorado. *Smithsonian Contributions to Paleobiology*, (27):87–93, 1976.
- Andrea Rotnitzky and Nicholas P. Jewell. Hypothesis testing of regression parameters in semiparametric generalized linear models for cluster correlated data. *Biometrika*, 77(3):485–497, 1990. ISSN 1464-3510. doi: 10.1093/biomet/77.3.485.
- Benjamin A. Shaby. The Open-Faced Sandwich Adjustment for MCMC Using Estimating Functions. *Journal of Computational and Graphical Statistics*, 23(3):853–876, September 2014. ISSN 1061-8600, 1537-2715. doi: 10.1080/10618600.2013.842174. URL <https://www.webofscience.com/api/gateway?GWVersion=2&SrcAuth=DOI&SrcApp=WOS&KeyAID=10.1080/10618600.2013.842174>. Web of Science ID: WOS:000338205400013.
- Kerryn E. Slack, Craig M. Jones, Tatsuro Ando, G. L.(Abby) Harrison, R. Ewan Fordyce, Ulfur Arnason, and David Penny. Early penguin fossils, plus mitochondrial genomes, calibrate avian evolution. *Molecular Biology and Evolution*, 23(6):1144–1155, March 2006. ISSN 0737-4038. doi: <https://doi.org/10.1093/molbev/msj124>.
- N. D. Smith. Phylogenetic analysis of peleciformes (aves) based on osteological data: implications for waterbird phylogeny and fossil calibration studies. *PLOS ONE*, 5(e13354), 2010.
- Mike Steel. A basic limitation on inferring phylogenies by pairwise sequence comparisons. *Journal of Theoretical Biology*, 256(3):467–472, February 2009. ISSN 0022-5193. doi: 10.1016/j.jtbi.2008.10.010. URL <https://www.sciencedirect.com/science/article/pii/S0022519308005390>.
- Koichiro Tamura, Fabia Ursula Battistuzzi, Paul Billing-Ross, Oscar Murillo, Alan Filipinski, and Sudhir Kumar. Estimating divergence times in large molecular phylogenies. *Proceedings of the National Academy of Sciences*, 109(47):19333–19338, November 2012. ISSN 1091-6490. doi: <https://doi.org/10.1073/pnas.1213199109>.
- Simon Tavaré. Some probabilistic and statistical problems in the analysis of dna sequences. *Lect Math Life Sci (am Math Soc)*, 17:57–86, 1986.
- Cristiano Varin. On composite marginal likelihoods. *Asta Advances in Statistical Analysis*, 92(1):1–28, February 2008. ISSN 1863-818X. doi: 10.1007/s10182-008-0060-7.
- Cristiano Varin, Nancy Reid, and David Firth. An overview of composite likelihood methods. *Statistica Sinica*, 21(1):5–42, 2011. ISSN 10170405, 19968507. URL <http://www.jstor.org/stable/24309261>.
- P. J. Waddell and M. A. Steel. General time-reversible distances with unequal rates across sites: Mixing gamma and inverse gaussian distributions with invariant sites. *Molecular Phylogenetics and Evolution*, 8(3):398–414, December 1997. ISSN 1055-7903, 1095-9513. doi: 10.1006/mpev.1997.0452. Web of Science ID: WOS:000071011300009.
- Jihua Wu and Edward Susko. General Heterotachy and Distance Method Adjustments. *Molecular Biology and Evolution*, 26(12):2689–2697, December 2009. ISSN 0737-4038. doi: 10.1093/molbev/msp184.
- Jihua Wu and Edward Susko. Rate-variation need not defeat phylogenetic inference through pairwise sequence comparisons. *Journal of Theoretical Biology*, 263(4):587–589, April 2010. ISSN 0022-5193. doi: 10.1016/j.jtbi.2009.12.022. URL <https://www.sciencedirect.com/science/article/pii/S0022519309005955>.
- Shaoyuan Wu, Frank E. Rheindt, Jin Zhang, Jiajia Wang, Lei Zhang, Cheng Quan, Zhiheng Li, Min Wang, Feixiang Wu, Yanhua Qu, Scott V. Edwards, Zhonghe Zhou, and Liang Liu. Genomes, fossils, and the concurrent rise of modern birds and flowering plants in the late cretaceous. *Proceedings of the National Academy of Sciences*, 121(8), February 2024a. ISSN 1091-6490. doi: 10.1073/pnas.2319696121.

Shaoyuan Wu, Frank E. Rheindt, Jin Zhang, Jiajia Wang, Lei Zhang, Cheng Quan, Zhiheng Li, Min Wang, Feixiang Wu, Yanhua Qu, Scott V. Edwards, Zhonghe Zhou, and Liang Liu. Reply to claramunt et al.: Robustness of the cretaceous radiation of crown aves. *Proceedings of the National Academy of Sciences*, 121(39), September 2024b. ISSN 1091-6490. doi: 10.1073/pnas.2412448121.

Yang Wu and Malay Ghosh. Asymptotic Expansion of the Posterior Based on Pair-wise Likelihood. *Sankhya-Series A-Mathematical Statistics and Probability*, 79(1):39–75, February 2017. ISSN 0976-836X, 0976-8378. doi: 10.1007/s13171-016-0094-y. URL <https://www.webofscience.com/api/gateway?GWVersion=2&SrcAuth=DOIISource&SrcApp=WOS&KeyAID=10.1007/s13171-016-0094-y>. Web of Science ID: WOS:000405820200003.

Wangang Xie, Paul O. Lewis, Yu Fan, Lynn Kuo, and Ming-Hui Chen. Improving marginal likelihood estimation for bayesian phylogenetic model selection. *Systematic Biology*, 60(2):150–160, December 2010. ISSN 1063-5157. doi: 10.1093/sysbio/syq085.

Z. Yang. Paml 4: Phylogenetic analysis by maximum likelihood. *Molecular Biology and Evolution*, 24(8):1586–1591, April 2007. ISSN 1537-1719. doi: <https://doi.org/10.1093/molbev/msm088>.

Z Yang and S Kumar. Approximate methods for estimating the pattern of nucleotide substitution and the variation of substitution rates among sites. *Molecular Biology and Evolution*, 13(5):650–659, May 1996. ISSN 0737-4038. doi: 10.1093/oxfordjournals.molbev.a025625.

Zh Yang. Maximum-Likelihood Phylogenetic Estimation from Dna-Sequences with Variable Rates Over Sites - Approximate Methods. *Journal of Molecular Evolution*, 39(3):306–314, 1994. ISSN 0022-2844. doi: 10.1007/BF00160154.

Ziheng Yang. *Molecular Evolution: A Statistical Approach*. Oxford University Press, 2014a.

Ziheng Yang. Bayesian computation (mcmc). pages 214–262, May 2014b. doi: <https://doi.org/10.1093/acprof:oso/9780199602605.003.0007>.

Ziheng Yang and Bruce Rannala. Bayesian estimation of species divergence times under a molecular clock using multiple fossil calibrations with soft bounds. *Molecular Biology and Evolution*, 23(1):212–226, September 2005. ISSN 0737-4038. doi: 10.1093/molbev/msj024.

Andrew D. Young and Jessica P. Gillung. Phylogenomics — principles, opportunities and pitfalls of big-data phylogenetics. *Systematic Entomology*, 45(2):225–247, December 2019. ISSN 1365-3113. doi: 10.1111/syen.12406.

Emile Zuckerkandl and Linus Pauling. Molecules as documents of evolutionary history. *Journal of Theoretical Biology*, 8(2):357–366, March 1965. ISSN 0022-5193. doi: 10.1016/0022-5193(65)90083-4. URL <https://www.sciencedirect.com/science/article/pii/0022519365900834>.

A Appendix: Supplementary Materials and Methods

A.1 Branch length estimation simulation

In the first simulation we estimate the branch lengths in mutation units, assuming an unrooted tree topology. Alignments are simulated under the *JC* and *GTR* substitution models, both with independent and identically distributed (iid) mutation rates at each site, and with variable rates distributed according to the Discrete Gamma distribution ($JC + \Gamma$, $GTR + \Gamma$) with 4 rate categories and rate parameter $\alpha = 0.5$ (Yang and Kumar, 1996). For each simulation setting, we generate 500 independent replicates.

We estimate the branch lengths after fixing the tree topology and substitution rate parameters at the true values. For the $GTR + \Gamma$, we also estimate the branch lengths after conducting a short MCMC run to estimate the relative rate and α parameters, and fixing the values to the posterior mean for the longer MCMC run used to estimate the branch lengths.

For the simulation settings described above, we assume the true substitution model parameters (including the site-rate heterogeneity parameter α) are known. In practice, these parameters may be estimated and fixed prior to estimating the branch lengths or node ages. We simulate applying this procedure to both the branch length and node age estimation simulations using the GTR substitution model with $\alpha = 0.5$. We conduct an initial MCMC run of 5000 generations with a burn-in of 1000 generations, in which only the substitution model parameters are sampled. The posterior mean is then fixed for the main MCMC run in which the branch lengths or node ages are sampled.

A.1.1 $GTR + \Gamma$ parameter estimation

For use of the PW and APW likelihoods, we assume the site rate heterogeneity parameter α is fixed. Additionally, the derivation of the adjustment weights for the APW1 and APW2 likelihoods assumes the substitution model parameters are fixed. We conduct additional branch length and node age estimation simulations using the $GTR + \Gamma$ substitution model in which we estimate the substitution model parameters from the data. For the PW, APW1, and APW2 likelihoods, we conduct a short initial MCMC run using the Full likelihood, from which estimates of the GTR relative rate parameters and α are obtained, and used to estimate the adjustment weight for the APW1 and APW2 cases. The estimate of α is then fixed, but the substitution model rate parameters are sampled during a main MCMC run to estimate the branch lengths or node ages. We compare these to estimates obtained by the Full likelihood in which all the $GTR + \Gamma$ parameters are sampled to ensure the estimates from the initial run are reasonable.

A.2 Fossil Calibrations

1. Split between lizard and chicken. Uniform(255.9, 299.8) prior distribution (Benton et al., 2009).
2. Split between *Paleognathae* and *Neognathae*. OLN(66.7, 81.3, 5.3), which uses *Asteriornis maasrichtensis* as the lower bound and *Ichthyornis dispar* as the ‘soft’ upper bound. (Field et al., 2018, 2020).
3. Stem *Corvidae*. OE(7.2, 50.6) based on fossil *Corvus larteri* (Milne-Edwards, 1867-1871).
4. Split between suboscines and oscines. OE(13.6, 53.8) based on fossil *Miocitta galbreathi* (Brodtkorb, 1972).
5. Stem *Psittaciformes*. OE(53.5, 73.8) based on fossil *Pulchrapollia gracilis* (Dyke and Cooper, 2000).
6. Stem *Strigiformes*. OE(56.8, 75.4) based on fossils *Berruornis orbisantiqui*, *Ogygoptynx wetmorei* (Mayr, 2002; Mourer-Chauviré, 1994; Rich and Bohaska, 1976).
7. Stem *Gruoidea*. OE(28.3, 61.2) based on fossil *Parvigrus pohli* (Mayr, 2005).
8. Stem *Apodiformes*. OE(51.58, 72.8) based on fossil *Eocypselus rowei* (Mayr, 2003; Ksepka et al., 2013).
9. Stem *Apodidae*. OE(48.4, 71.2) based on fossil *Scaniacypselus wardi* (Ksepka et al., 2013; Mlíkovský, 2002).
10. Stem *Steatornithidae*. OE(51.58, 72.8) based on fossil *Prefica nivea* (Olson, 1987; Nesbitt et al., 2011; Mayr, 2005; Harrison, 1984).
11. Stem *Sphenisciformes*. OE(60.5, 77.3) based on fossil *Waimanu manneringi* (Slack et al., 2006).
12. Stem *Fregitidae*. OE(51.58, 72.8) based on fossil *Limnofregata azygosternon* (Olson, 1977; Smith, 2010).

13. Stem *Threskiornithidae*. OE(53.9, 74) based on fossil *Rhynchaetes* (Mayr and Bertelli, 2011).
14. Stem *Phaethontidae*. OE(55.6, 74.8) based on fossil *Lithoptila abdouensis* (Bourdon et al., 2005).
15. Stem *Musophagidae*. OE(51.58, 72.8) based on fossil *Foro panarium* (Field and Hsiang, 2014; Olson, 1992).
16. Stem *Coliiformes*. OE(56.22, 75.2) based on fossil *Sandcoleus copiosus* (Houde and Olson, 1992; Ksepka, 2009).
17. Stem *Coraciidae* and *Brachypteraciidae*. OE(51.57, 72.8) based on fossil *Primobucco mcgreui* (Ksepka and Clarke, 2010; Brodkorb, 1972; Clarke et al., 2009).
18. Stem *Pici*. OE(28.3, 61.2) based on fossil *Rupelramphastoides knopfi* (Mayr, 2005, 2006b).
19. Stem *Upupidae* and *Phoeniculidae*. OE(46.6, 70.3) based on fossil *Messelirrisor grandis* (Mayr, 2000, 2006a).
20. Stem *Galliformes*. OE(51.58, 72.8) based on fossil *Gallinuloides wyomingensis* (Ksepka, 2009).

A.3 Bird Tree Topology

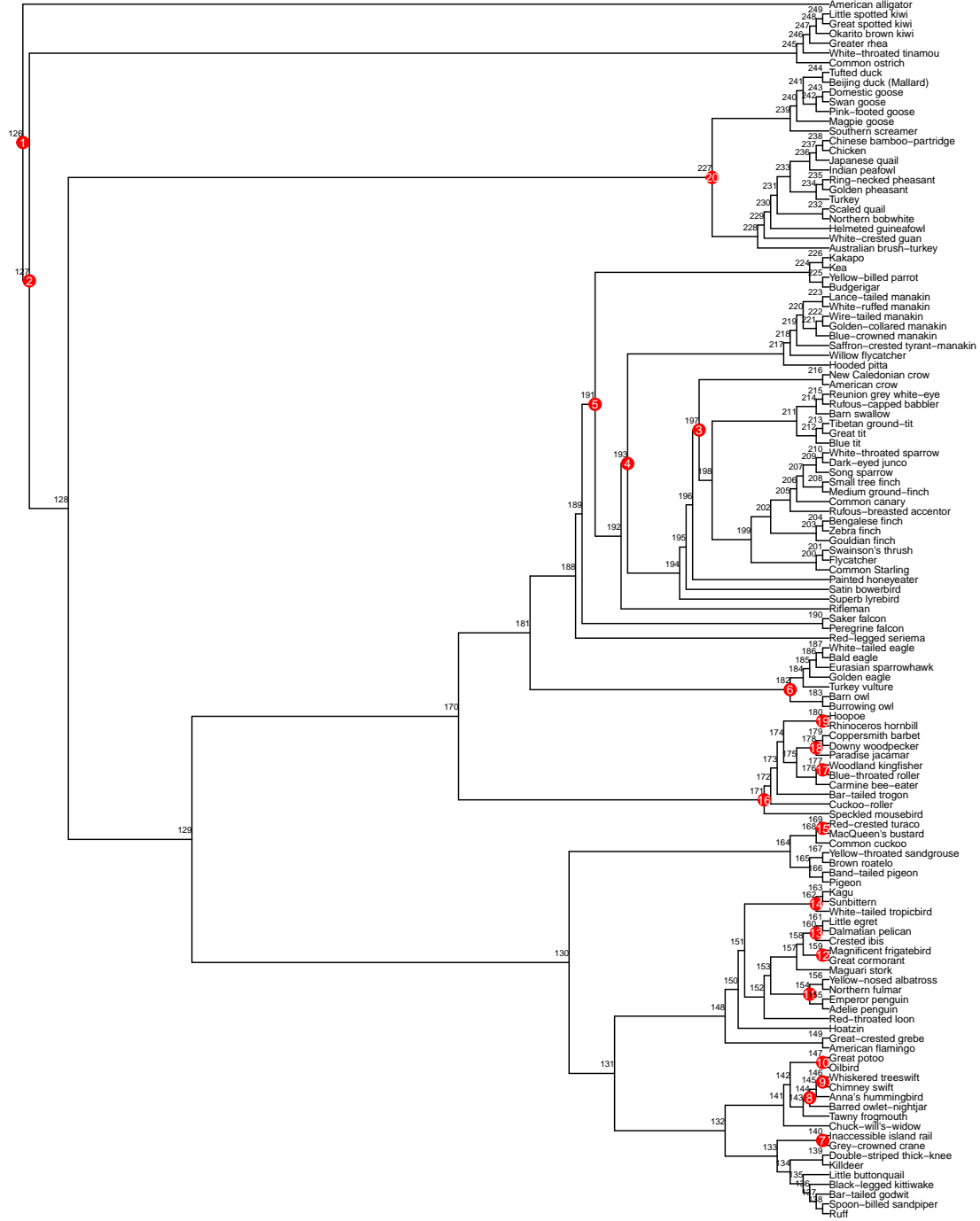


Figure 7: Tree topology estimated from 100 concatenated genes. Nodes calibrated by fossil information are indicated by red points.

B Appendix: Supplementary Results

Likelihood	Sub Mod	rMSE			CI Coverage		
		Sites			Sites		
		1000	10000	100000	1000	10000	100000
Full	<i>JC</i>	0.007450	0.002343	0.001090	0.932	0.937	0.931
PW	<i>JC</i>	0.007414	0.002391	0.001122	0.865	0.868	0.860
APW1	<i>JC</i>	0.007378	0.002388	0.001125	0.976	0.979	0.976
APW2	<i>JC</i>	0.007913	0.002491	0.001137	0.995	0.997	0.996
Full	<i>JC</i> + Γ	0.010303	0.003048	0.001420	0.935	0.938	0.936
PW	<i>JC</i> + Γ	0.010644	0.003255	0.001521	0.873	0.879	0.876
APW1	<i>JC</i> + Γ	0.010524	0.003274	0.001515	0.976	0.986	0.986
APW2	<i>JC</i> + Γ	0.012393	0.003725	0.001750	0.992	0.999	0.999
Full	<i>GTR</i>	0.008081	0.002384	0.001076	0.935	0.935	0.930
PW	<i>GTR</i>	0.007877	0.002432	0.001116	0.866	0.868	0.863
APW1	<i>GTR</i>	0.007864	0.002436	0.001120	0.972	0.980	0.978
APW2	<i>GTR</i>	0.008503	0.002577	0.001130	0.993	0.997	0.997
Full	<i>GTR</i> + Γ	0.010928	0.003244	0.001513	0.931	0.936	0.933
PW	<i>GTR</i> + Γ	0.010779	0.003367	0.001600	0.868	0.876	0.870
APW1	<i>GTR</i> + Γ	0.010787	0.003401	0.001600	0.973	0.984	0.985
APW2	<i>GTR</i> + Γ	0.012566	0.003998	0.001856	0.991	0.998	0.999

Table 2: Simulation node age estimation results. The bottom three rows show the results of the node age estimation when the *GTR* rate parameters are estimated simultaneously (Full likelihood) or estimated with a short run using the full likelihood and fixed for subsequent analysis (Pairwise, Adjusted Pairwise)

			rMSE			CI Coverage		
			Sites			Sites		
Likelihood			1000	10000	50000	1000	10000	50000
Branch Lengths	Full		0.01106	0.00356	0.00151	0.94	0.94	0.93
	PW		0.01109	0.00375	0.00159	0.89	0.89	0.87
	PWA1		0.01110	0.00370	0.00162	0.98	0.99	0.98
	PWA2		0.02885	0.00817	0.00311	0.98	1.00	1.00
			Sites			Sites		
Likelihood	ν Fixed		1000	10000	50000	1000	10000	50000
Node Ages	Full	No	3.51	2.50	2.40	0.97	0.99	0.97
	Full	Yes	3.45	2.44	2.31	0.98	0.98	0.98
	PW	No	3.60	2.91	3.06	0.97	0.95	0.86
	PW	Yes	3.56	2.73	3.22	0.98	0.98	0.89
	PWA1	No	3.37	2.71	3.02	0.99	0.98	0.94
	PWA1	Yes	3.40	2.66	2.72	0.99	0.99	0.98
	PWA2	No	2.23	1.80	1.91	1.00	1.00	1.00
	PWA2	Yes	2.33	1.78	1.92	1.00	1.00	1.00

Table 3: Results for simulations where *GTR* + Γ parameters (ν) are estimated from the data. The top region of the table shows the results of branch length estimation in mutation units. The bottom region shows the results of the node age estimation. For the node age estimation setting, the ' ν Fixed' column indicates whether the *GTR* + Γ parameters are fixed after the initial MCMC run or sampled during the main MCMC run.

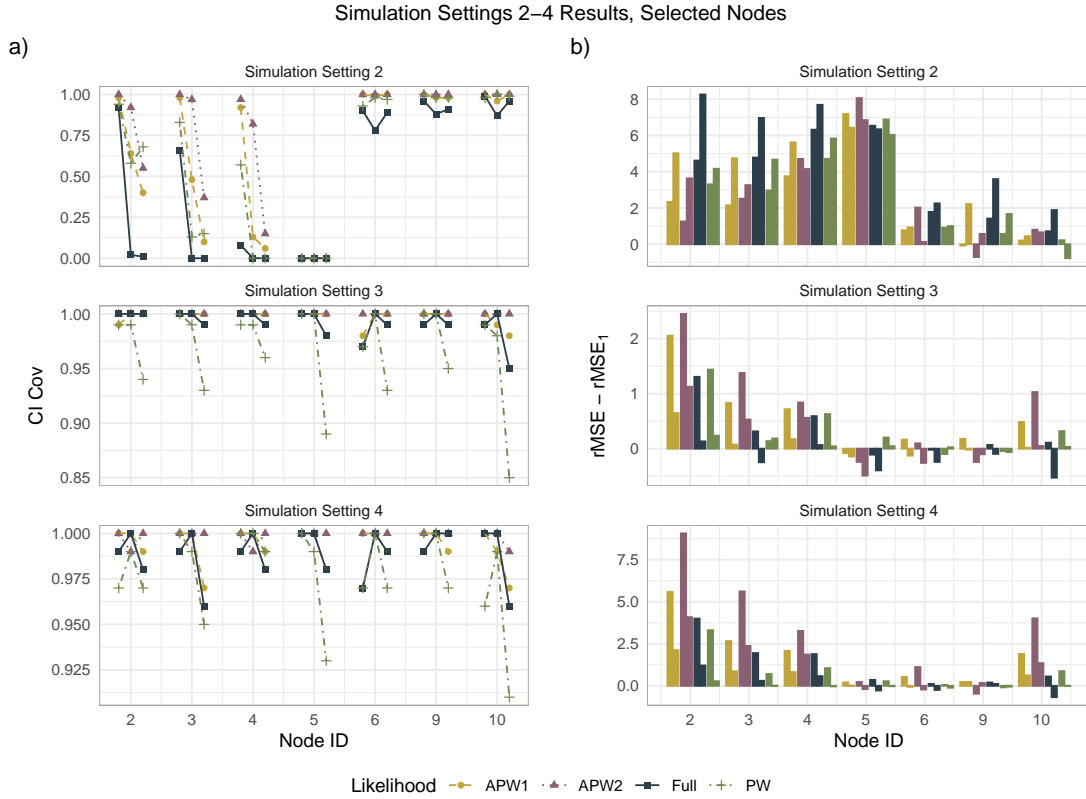


Figure 8: Node-wise CI results for Simulations 2-4, selected nodes.

a) Node-wise CI Coverage for Calibration Settings 2-4.

b) Node-wise difference in rMSE between Calibration Settings 2-4 and Setting 1.

For each node, there are 2 bars for each likelihood that represent (from left to right) the 1000 site and 10,000 settings.

Setting 5-7 Results, Selected Node

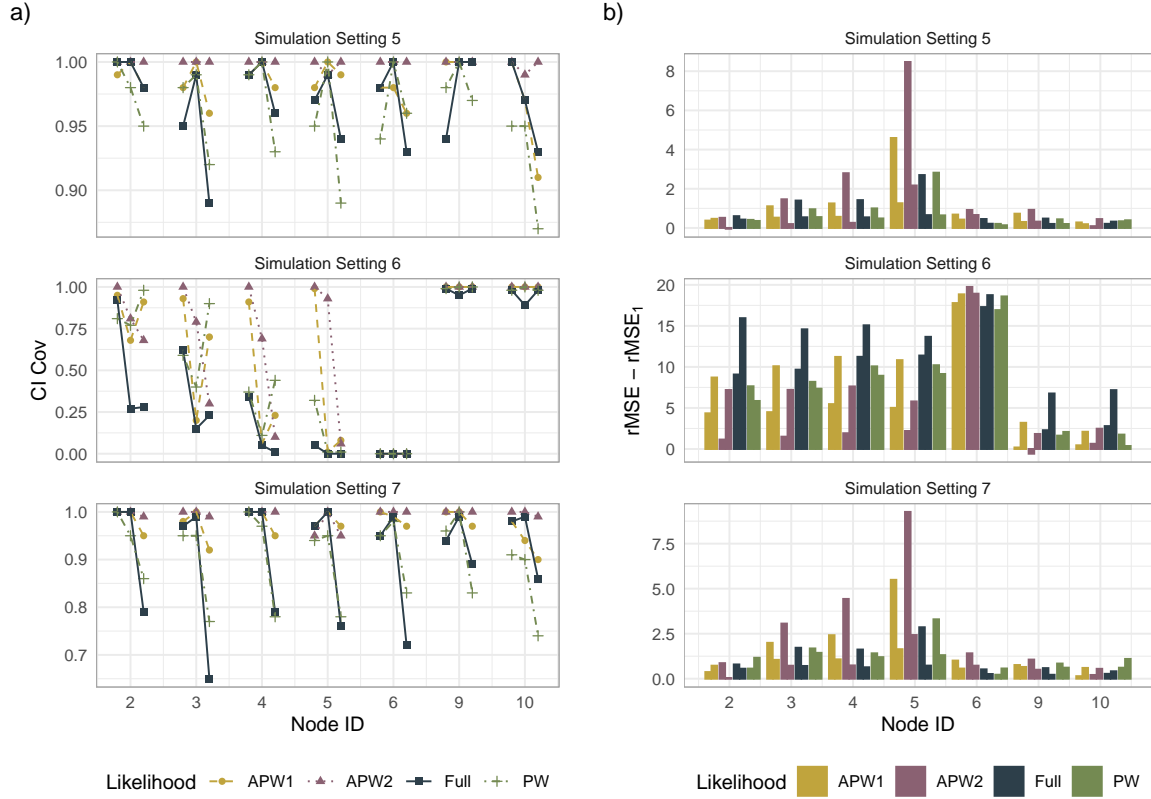


Figure 9: Node-wise CI results for Simulations 5-7, selected nodes.

a) Node-wise CI Coverage for Calibration Settings 5-7.

b) Node-wise difference in rMSE between Calibration Settings 5-7 and Setting 1.

For each node, there are 2 bars for each likelihood that represent (from left to right) the 1000 site and 10,000 settings.

Parameter	Full Likelihood Run	Initial Run
r_{AC}	0.0812	0.0822
r_{AG}	0.3670	0.3278
r_{AT}	0.0437	0.0445
r_{CG}	0.1122	0.1116
r_{CT}	0.3706	0.3697
r_{GT}	0.0652	0.0653
α	0.4495	0.4525

Table 4: $GTR + \Gamma$ parameters estimated from Full likelihood run and fixed for PW likelihoods using a short initial run.

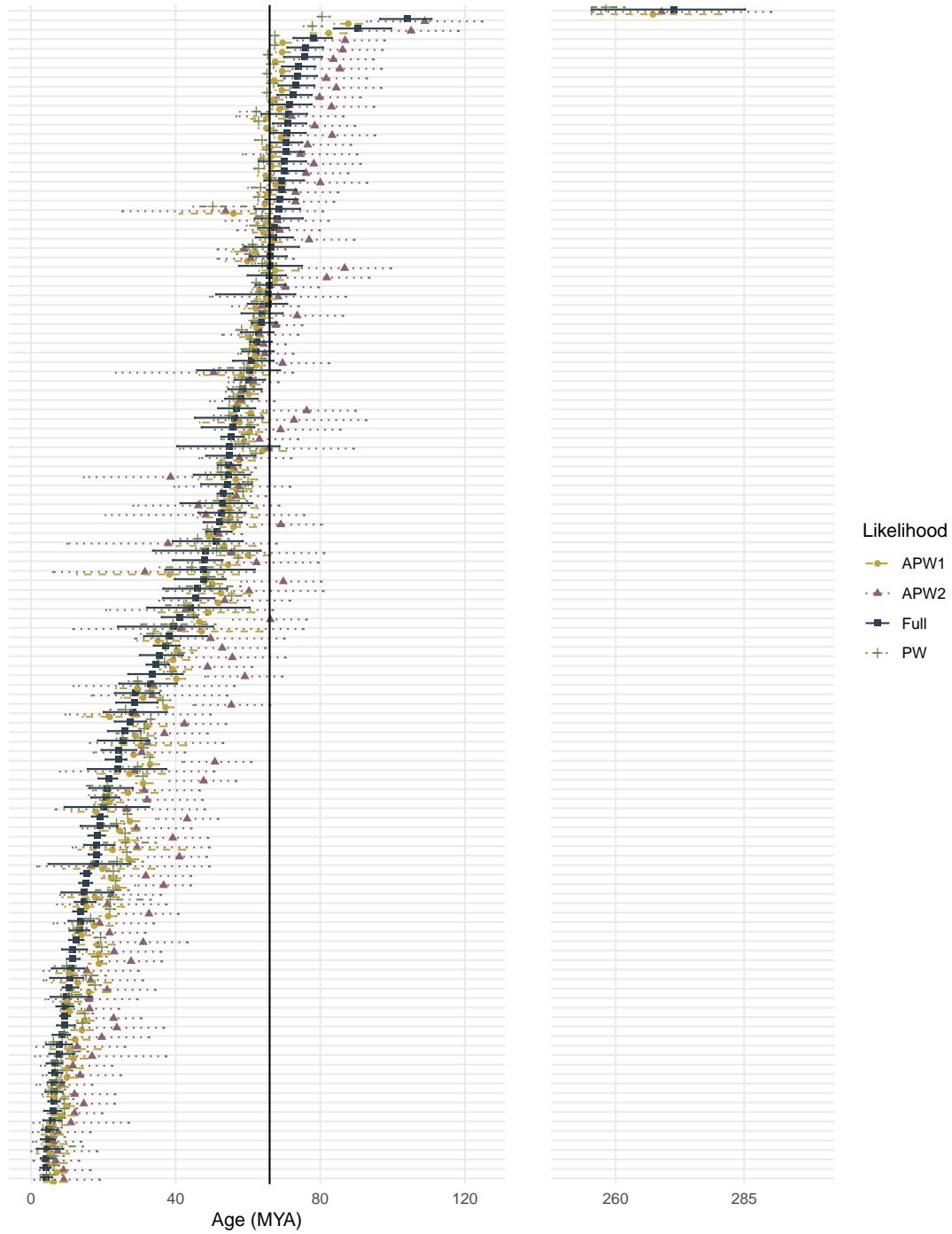


Figure 10: Node age estimates for all nodes of bird tree topology. The APW1, APW2, Full, and PW likelihood-based point estimates are indicated by the yellow circles, red triangles, black squares, and green crosses, respectively. The corresponding 95% credible intervals are given by the yellow dashed, green dotted, black solid, and green dot-dashed lines, respectively.

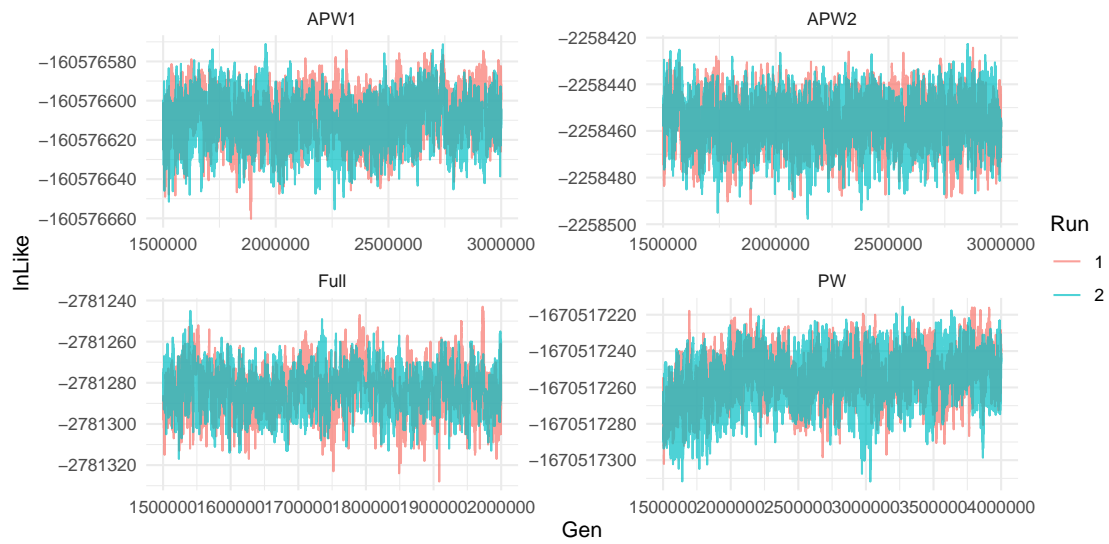


Figure 11: Trace plots showing log likelihood values for two independent runs per likelihood.